

AD 663717

AFCRL-67-0621  
NOVEMBER 1967  
AIR FORCE SURVEYS IN GEOPHYSICS, NO. 199



**AIR FORCE CAMBRIDGE RESEARCH LABORATORIES**  
L. G. HANSCOM FIELD, BEDFORD, MASSACHUSETTS

**Radio Astronomy: A Revision of  
Chapter 22, Handbook of Geophysics  
and Space Environments**

D.A. GUIDICE

DDC  
RECEIVED  
JAN 15 1968  
RECEIVED  
C

**OFFICE OF AEROSPACE RESEARCH**  
**United States Air Force**



AFCRL-67-0621  
NOVEMBER 1967  
AIR FORCE SURVEYS IN GEOPHYSICS, NO. 199

ENVIRONMENTAL CONSULTATION SERVICE

**AIR FORCE CAMBRIDGE RESEARCH LABORATORIES**

L. G. HANSCOM FIELD, BEDFORD, MASSACHUSETTS

**Radio Astronomy: A Revision of  
Chapter 22, Handbook of Geophysics  
and Space Environments**

D.A. GUIDICE

Distribution of this document is unlimited. It may be released to the Clearinghouse, Department of Commerce, for sale to the general public.

**OFFICE OF AEROSPACE RESEARCH**  
**United States Air Force**



## Abstract

This survey is a summary of available information on radiation environments at radio frequencies (about 10 m to 1 cm wavelength); the Moon, the Planets, and space beyond the solar system are described. The topics presented are refraction and absorption of extraterrestrial radio waves by the Earth's atmosphere, radio and radar observations of the Moon and Planets, radio emission from the celestial sphere (background radiation), discrete sources of continuum radio emission, and spectral-line radiation from neutral atomic hydrogen and from the hydroxyl radical (OH).

## Contents

22.1	FUNDAMENTAL CONCEPTS AND DEFINITIONS	1
22.2	EFFECTS OF THE EARTH'S ATMOSPHERE	6
22.2.1	Refraction	6
22.2.2	Scintillation	6
22.2.3	Absorption	7
22.3	RADIO CHARACTERISTICS OF THE MOON AND PLANETS	9
22.3.1	Radio Emission of the Moon	9
22.3.2	Radio Emission of the Planets	11
22.3.2.1	Mercury	12
22.3.2.2	Venus	12
22.3.2.3	Mars	13
22.3.2.4	Jupiter	13
22.3.2.5	Saturn	14
22.3.2.6	Uranus	14
22.3.3	Radar Observations of the Moon	14
22.3.4	Radar Observations of the Planets	15
22.4	MAPS OF BACKGROUND RADIATION	17
22.5	DISCRETE SOURCES OF RADIO EMISSION	17
22.5.1	Flux Densities and Spectra	17
22.5.2	Sources With Large Variations in Flux Density	33
22.6	SPECTRAL LINE RADIATION	34
22.6.1	The 21-cm Atomic Hydrogen Line	35
22.6.2	Excited-State Hydrogen Lines	35
22.6.3	The 18-cm Hydroxyl (OH) Lines	35
22.7	REFERENCES	36
	APPENDIX B: Blackbody Radiation	B-1

## Illustrations

22-1. Attenuation by combined water vapor and oxygen calculated from measurements	8
22-2. Relative return-power from the lunar surface as a function of the angle of incidence of the radar signal	16
22-3. Galactic radio emission at 38 MHz	18-19
22-4. Background radiation at 81 MHz	20
22-5. Background radiation at 250 MHz	20
22-6. Background radiation at 400 MHz	21-28
22-7. Background radiation at 960 MHz	30
22-8. The spectra of the five strongest radio sources	31
22-9. The spectra of various types of discrete radio sources	33
22-10. Shape of the spectrum of three variable radio sources compared with that of the normal nonthermal source Virgo A	34
22-11. Energy levels, rest-frequencies, and relative line intensities (theoretical) for the $^2\Pi_{3/2}$ , $J = 3/2$ state of OH	36
B-1. Spectral radiance of a blackbody at various temperatures	B-4
B-2. Radiance per reciprocal centimeter and radiance per unit frequency for a blackbody at various temperatures	B-5
B-3. Spectral radiance and radiance per reciprocal centimeter of blackbodies at various temperatures plotted on arithmetic scales	B-6
B-4. Radiance per unit frequency for blackbodies at high temperatures vs frequency	B-7
B-5. Number of photons per second emitted per square centimeter per steradian per micron by a blackbody at various temperatures	B-8
B-6. Number of photons per second per square centimeter per steradian per reciprocal centimeter and number of photons per second per square centimeter per steradian per unit frequency emitted by a blackbody at various temperatures	B-9
B-7. Photons per second emitted by blackbodies at various temperatures plotted on arithmetic scales	B-10

## Tables

22-1. Experimental Brightness-Temperature Parameters of the Moon	11
22-2. Equivalent Blackbody Temperatures of Planets	13
22-3. Relative Radar Cross Sections of the Moon	15
22-4. Positions and Angular Diameters of the Brightest Discrete Radio Sources	32
22-5. Flux Densities of the Brightest Discrete Radio Sources	32

## Preface

This report is a revision of Sections 22.3 through 22.7 of Chapter 22, "Radio Astronomy" of the Handbook of Geophysics and Space Environments; \* changes in Sections 22.1 and 22.2 are minor. (Numbers for Sections and Subsections are the same as those in the original Handbook, so that the cross-referencing system in other chapters remains valid.) The information available in the literature through December 1966 is covered. This survey represents the state of the art in the spring of 1967, when the manuscript was completed.

A corrected copy of Appendix B, "Blackbody Radiation", of the Handbook is included with this survey because the subject is basic in studies of radiation; in addition some recipients of this survey may not have the errata issued for the Handbook of Geophysics and Space Environments.

SHEA L. VALLEY  
Scientific Editor  
Handbook of Geophysics and Space Environments

---

\*Published by the Air Force Cambridge Research Laboratories and by the McGraw-Hill Book Co. in 1965.

## Radio Astronomy: A Revision of Chapter 22, HANDBOOK OF GEOPHYSICS AND SPACE ENVIRONMENTS

Radio astronomy is the branch of astronomy concerned with the reception of radiation at radio wavelengths from extraterrestrial sources. In this chapter, sources other than the sun are described; for solar radio astronomy, see Chapter 16.

Many types of radio telescopes are in use; they include steerable and fixed paraboloids, cross arrays, and multi-element interferometers. The trend in design responds to three main astronomical requirements: increased collecting area for the study of faint sources, increased angular resolution for accurate position finding and fine mapping, and increased precision in antenna pointing. For descriptions of the various types see Wild [1966].

### 22.1 FUNDAMENTAL CONCEPTS AND DEFINITIONS

All observations in radio astronomy consist of the measurement of an antenna temperature and the conversion of that temperature to a measure of power received from the source. The antenna temperature,  $T_A$ , is the measure of the power in the radiation accepted by the antenna. The antenna receives power,  $P_A$ , equivalent to that from a resistor at the temperature  $T_A$ . The defining equation is

$$P_A = k T_A \Delta f , \quad (22-1)$$

where  $k$  is Boltzmann's constant ( $1.38 \times 10^{-23} \text{ J } ^\circ\text{K}^{-1}$ ),  $\Delta f$  is the bandwidth in cycles per second (Hz),  $T_A$  is in degrees Kelvin, and  $P_A$  is in watts.

The terms equivalent, or apparent, blackbody temperature, used to describe a radio source, mean that the radiation received is of the same magnitude as that which would be received from an ideal radiator (blackbody) at this temperature, subtending the same solid angle as the source producing the observed radiation. The temperature of the source may be of thermal or unknown origin; only if the source radiates as a true blackbody will its physical temperature equal the apparent blackbody temperature. Definitions, formulas, and curves for blackbody radiation are given in Appendix B. The Rayleigh-Jeans approximation for blackbody radiation at radio frequencies is used throughout this chapter.

In any electrical conductor or resistor there are small voltage fluctuations due to internal random motion. The continuous random (thermal) motion of electrons and ions is the equivalent of random varying electric currents; the moving charges radiate electromagnetic waves at all frequencies. The power in these thermal fluctuations, or Johnson noise, from a matched resistor at temperature  $T$  is

$$P = k T \Delta f . \quad (22-2)$$

The resistor is connected to an antenna where the radiation impedance is the same as the resistor; the connection is made through a transmission line that is lossless and matched to the resistor and antenna. Then, if the antenna is surrounded by a blackbody at the same temperature as the resistor, the thermal radiation from the blackbody will be transmitted to, and completely absorbed by, the resistor. Johnson noise in the resistor will be transferred to, and completely absorbed by, the blackbody. Since the temperatures of the resistor and the blackbody are equal, the power from each is the same. For Johnson noise the power per unit bandwidth is independent of the frequency.

The brightness (radiance) per unit bandwidth,  $B_f$ , is proportional to the square of the frequency;

$$B_f = 2k T_b f^2 / c^2 = 2k T_b / \lambda^2 \text{ [ W m}^{-2} \text{ sr}^{-1} \text{ Hz}^{-1} \text{ ]} , \quad (22-3)$$

where  $T_b$  is the brightness (blackbody) temperature of the source,  $c$  is the velocity of light in vacuum, and  $\lambda$  is the wavelength. Thermodynamic balance of the two sources of noise is achieved because, as the frequency increases, the antenna accepts radiation from a solid angle  $\Omega_A$ , or has an effective area  $A_e$ , that is proportional to  $1/f^2$  [see Eq. (22-14)]. When the product of brightness per unit bandwidth and the antenna effective area is integrated over the antenna solid angle, the  $f^2$  terms cancel. The power per unit bandwidth,  $w$ , is the spectral power; the general formula is

$$w = \frac{1}{2} A_e \iint_{4\pi} B_f(\theta, \phi) F_n(\theta, \phi) d\Omega \quad , \quad (22-4)$$

where  $1/2$  is the polarization factor,  $B_f(\theta, \phi)$  is the brightness function, and  $F_n(\theta, \phi)$  is the normalized power pattern of the antenna, normalized so that  $F_{\max}(\theta, \phi) = 1$ . For a blackbody at constant temperature,  $B_f(\theta, \phi)$  is given by Eq. (22-3), so  $w$  is  $(1/2) A_e (2kT/\lambda^2) \Omega_A$ ; hence, using Eq. (22-14), the spectral power of a blackbody is  $kT$ . Thus, an antenna surrounded by or immersed in a blackbody reservoir at a constant temperature will have a constant power output per unit bandwidth that is independent of frequency.

In the case of actual observations, the antenna is not surrounded by a constant temperature background because the sky temperature varies with the direction in which the antenna is pointing. Therefore, temperature and brightness are functions of position coordinates  $\theta$  and  $\phi$ ;

$$B_f(\theta, \phi) = 2kT(\theta, \phi)/\lambda^2 \quad . \quad (22-5)$$

For a source of radiation that subtends a very small solid angle  $\Omega_{sm}$  with average brightness temperature  $T_s$  over the solid angle of the source, the flux density (power per unit bandwidth per unit area) is

$$S = 2kT_s \Omega_{sm} / \lambda^2 \quad [W m^{-2} Hz^{-1}] \quad . \quad (22-6)$$

The apparent flux density,  $S_A$ , of a source of constant brightness temperature  $T_s$  subtending a solid angle  $\Omega_s$  that is not small compared to the solid angle of the antenna is

$$S_A = 2kT_A / A_e \quad . \quad (22-7)$$

The true flux density of such a source is

$$S = 2kT_A L / A_e \quad , \quad (22-8)$$

where  $L$  is an antenna correction factor  $\frac{\Omega_s}{\iint_{\text{source}} F_n(\theta, \phi) d\Omega}$ ,

which must be used when  $\theta_h$ , the antenna half-power beamwidth, is less than five times the angular diameter of the source. For  $\theta_h$  greater than five times the angular diameter of the source,  $L$  approaches unity and the apparent flux density, Eq. (22-7), is essentially the true flux density.

The antenna temperature due to a discrete source, excluding the background sky temperature, is

$$T_A = A_e \Omega_s T_s / \lambda^2 = T_s \Omega_s / \Omega_A , \quad (22-9)$$

or

$$T_A = \eta_\Omega T_s \Omega_s / \Omega_M ; \quad (22-10)$$

$\Omega_M$  is the solid angle of the antenna main lobe and  $\eta_\Omega$  is the antenna beam efficiency. The beam efficiency is the measure of the concentration of radiated power in the region of the main lobe;  $\eta_\Omega = \Omega_M / \Omega_A$ . The stray factor,  $1 - \eta_\Omega$ , is indicative of the power in the antenna side lobes.

If  $\Omega_M$  is taken as the solid angle to first minimum, for a Gaussian beam pattern (with circular symmetry)

$$\Omega_M = 1.113 \theta_h^2 \quad [\text{sr}] , \quad (22-11)$$

and for a Bessel-function beam pattern

$$\Omega_M = 1.008 \theta_h^2 \quad [\text{sr}] , \quad (22-12)$$

where  $\theta_h$ , the half-power beamwidth, is in radians. (If  $\theta_h$  is given in angular degrees, divide the right-hand side of Eq. (22-11) or Eq. (22-12) by 3280 to obtain  $\Omega_M$  in steradians.) Ordinarily, the half-power beamwidths in the orthogonal planes (often referred to as the E and H planes, according to the polarization alignment of the feed) are determined experimentally by drifts or scans through a "point" source. For an antenna with circular symmetry, a simple approximation is

$$\theta_h = 70 \lambda / d \quad [\text{angular degree}] , \quad (22-13)$$

where  $d$  is the diameter of the physical aperture in the same length unit as  $\lambda$ .

The antenna solid angle,  $\Omega_A$ , is defined as that solid angle through which the total power radiated by the antenna would flow if the radiation were uniform and equal to its maximum intensity over this angle;

$$\Omega_A = \lambda^2 / A_e = \iint_{4\pi} F_n(\theta, \phi) d\Omega . \quad (22-14)$$

The aperture efficiency of an antenna is

$$\xi_A = A_e / A_{\text{phy}} , \quad (22-15)$$

where  $A_{\text{phy}}$  is the physical area of the aperture.

The directivity of an antenna is

$$D = 4\pi / \Omega_A = 4\pi A_e / \lambda^2 . \quad (22-16)$$

The gain of an antenna is

$$G = \eta_r D ; \quad (22-17)$$

$\eta_r$ , the radiation efficiency, is taken as equal to one for most antennas used in radio astronomy. (The ohmic loss on most radio telescopes is negligible).

A fundamental formula for antenna temperature is

$$T_A = \frac{1}{4\pi} \iint_{4\pi} T(\theta, \phi) D(\theta, \phi) d\Omega , \quad (22-18)$$

where  $T(\theta, \phi)$  is the sky brightness temperature distribution,  $D(\theta, \phi)$  is the antenna directivity function, and  $d\Omega$  is  $\sin \theta d\theta d\phi$ . The directivity defined in Eq. (22-16) is the directivity along the pointing axis of the radio telescope, that is, the maximum directivity. Thus,

$$D(\theta, \phi) = D F_n(\theta, \phi) = (4\pi / \Omega_A) F_n(\theta, \phi) . \quad (22-19)$$

The antenna temperature of a source can be found by the differential method, using various scanning techniques. In the drift technique the antenna is kept stationary and the source passes through the antenna beam as the earth rotates. If  $T_s(\theta, \phi)$  is the brightness temperature distribution of the source,

$$T_A = \frac{\eta_r \Omega}{\Omega_M} \iint_{\text{source}} T_s(\theta, \phi) F_n(\theta, \phi) d\Omega . \quad (22-20)$$

A discrete source of large flux density can be used to determine the normalized antenna pattern; for a "point" source in a region of uniform background brightness, the scan, or drift, curve directly yields the power pattern of the antenna. For the frequency range 100 to 3000 MHz this technique is often used as a method of calibrating a large steerable antenna used for purposes other than radio astronomy (for example, radar, communications, and so forth). (A number of useful radio sources and their flux densities as a function of frequency are described in Sec. 22.5.)

An equatorial antenna mount is constructed so that one scan-axis is perpendicular to, and one parallel to, the earth's axis of rotation. With such a mount one can operate directly in terms of the astronomical coordinates of right ascension and declination. A coordinate converter is often used with an elevation-azimuth mount so that the observer can still operate his program in astronomical coordinates. The coordinate converter translates operations in right ascension and declination into elevation and azimuth drive-commands.

## 22.2 EFFECTS OF THE EARTH'S ATMOSPHERE

### 22.2.1 Refraction

The refraction of electromagnetic waves in the lower atmosphere is determined by the dry-air pressure, the water vapor content, and the temperature (see Chapter 9). Refraction in the upper atmosphere is determined by the electron distribution in the ionosphere at heights from 80 to 1000 km. There is greater refraction at dekameter and meter wavelengths than in the microwave region because the index of refraction of the ionosphere varies inversely with the square of the frequency. In general, the refraction decreases as altitude increases. Because of local irregularities, however, refraction at a given elevation may be slightly greater in some cases than at a lower angle; there are variations from day to day and during the course of one day.

### 22.2.2 Scintillation

The amplitude of radio-frequency signals received from a discrete source (Sec. 22.5) of small angular diameter is not steady but exhibits considerable changes in intensity. This fluctuation is called scintillation. Signals from sources of large angular diameter do not scintillate. (This effect is familiar in the visible region; stars twinkle whereas planets usually do not.) Scintillation of radio-frequency signals is caused by irregularities in the ionosphere or troposphere; the motion (relative to the detector) of regions in which the local index of refraction differs from the surrounding medium causes fluctuations in the signal received.

At microwave frequencies, scintillations result from local variations in the refractive index of the troposphere; these scintillations have a relatively long period. At metric and dekametric wavelengths, scintillations result from variations in the ionosphere; local irregularities in electron density cause variations in refractive index at these wavelengths. The period of ionospheric scintillations is usually the order of a few seconds to one or two minutes.

The antenna beam has a much longer viewing path through the ionosphere at low angles of observation, so that at frequencies from 20 to 100 MHz ionospheric scintillations are frequently present at elevations less than five degrees.

In general, the amplitude of the scintillations varies inversely with some power (between 1 and 2) of the frequency, thus scintillations at higher frequencies are much less noticeable than at lower frequencies. Scintillations caused by weak scattering are well correlated at different frequencies over a large frequency range; hence, they probably result from single scattering by a region of different electron density than the surrounding medium.

The amplitude and the number (or frequency of occurrence) of ionospheric scintillations depends on magnetic activity. On occasion, during periods of intense magnetic disturbance, an inversion occurs; the higher frequency records show more scintillation than the lower frequency records. These scintillations show a phase difference in the signals at different frequencies; therefore, the inversion is probably the result of multiple scattering.

### 22.2.3 Absorption

Energy from radio sources is absorbed by molecular oxygen and water vapor in the lower atmosphere. In general, the absorption is much greater at millimeter wavelengths than at the longer wavelengths. At the wavelengths of resonant spectral lines, or of groups of lines forming an absorption band, the atmospheric absorption is very strong, as great as 10 dB per km. An example of an absorption band is the 60 GHz oxygen band which consists of a series of about 25 individual spectral lines that are pressure-broadened at lower and intermediate altitudes in the troposphere to form strong absorption from 54 to 66 GHz. At wavelengths of 1.25 cm, 1.63 mm, 0.9 mm, and shorter, the very strong absorption is due to water vapor. Around 5 mm and at 2.5 mm the very strong absorption is due to molecular oxygen. Figure 22-1 shows horizontal atmospheric attenuation as a function of frequency for two altitudes.

The amount of attenuation of the energy from a radio source in space depends on the altitude and the zenith angle at which the energy is received and on the temperature and the water vapor content of the atmosphere. The higher the altitude of the receiving site, the lower the attenuation. The attenuation, in dB, for zenith angles less than  $75^\circ$  varies as a function of the secant of the zenith angle,  $\zeta$  :

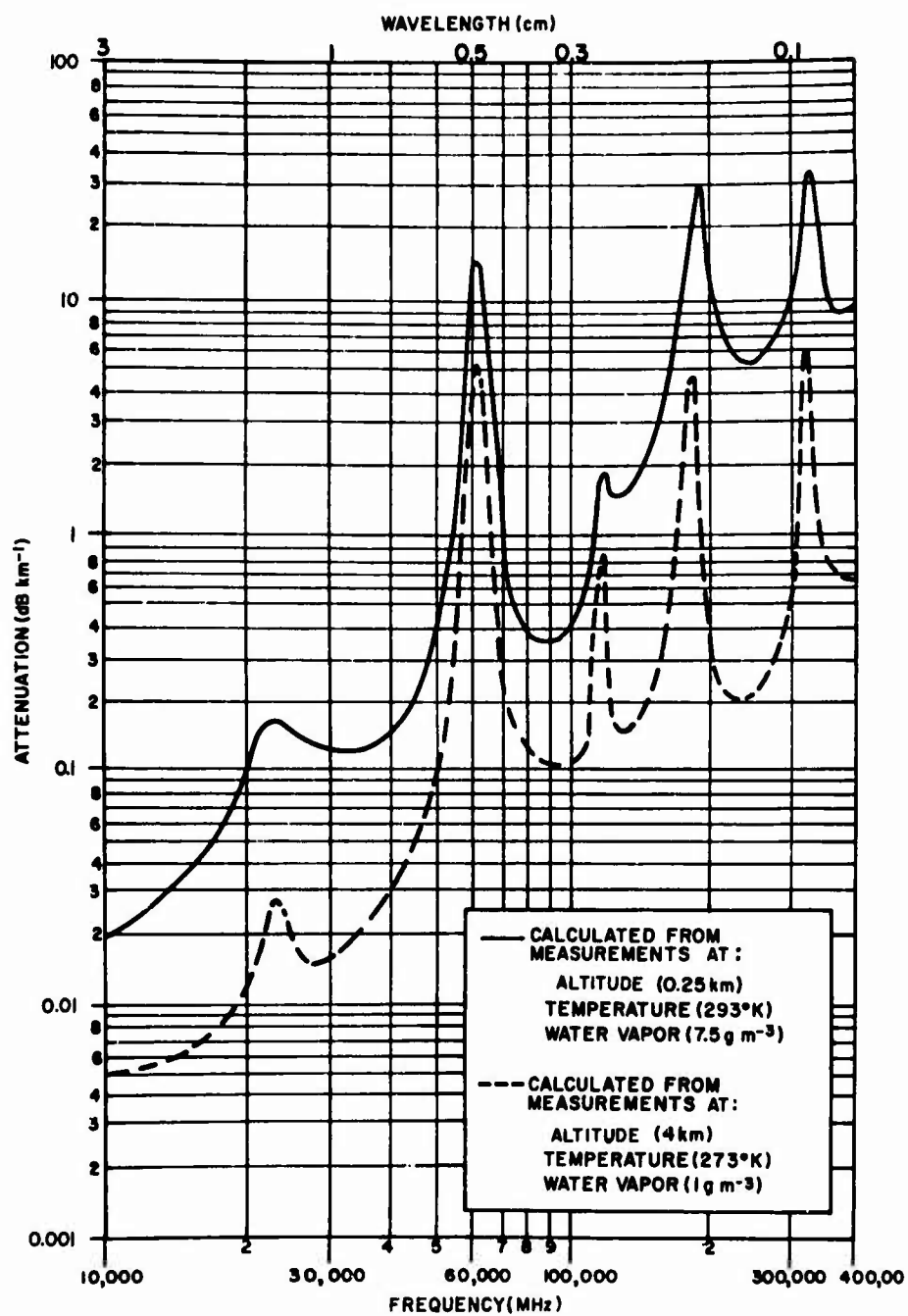


Figure 22-1. Attenuation by combined water vapor and oxygen calculated from measurements. (After C.W. Tolbert, A.W. Straiton, J.H. Douglas, Electrical Engineering Lab. Rept No. 104, University of Texas, 1958).

$$A(\xi) = A_v \sec \xi \quad [\text{dB}] \quad , \quad (22-21)$$

where  $A_v$  is the vertical (zenith angle zero) attenuation in dB. Attenuation is increased by an increase in the temperature or the water vapor content of the atmosphere.

The absorption of radio frequency energy by the ionosphere becomes important for dekameter and longer wavelengths. Ionospheric absorption shows large variations, and depends upon latitude, local time, season, and solar activity. The greatest absorption occurs in the daytime; absorption is minimum from midnight to 0500 local time. The strongest absorption takes place in the D region, which is present only during the daylight hours. D-region absorption is proportional to  $(f + f_L)^{-2}$ , where  $f$  is the frequency of the operating signal and  $f_L$  is the longitudinal component of the electron gyrofrequency. At night absorption takes place in the F region; this is generally much weaker than D-region absorption. In addition to the normal ionospheric absorption, drastic absorption events occur. These events are associated with solar flares and related geomagnetic disturbances; examples are polar-cap absorption and auroral-zone absorption. For further information on ionospheric phenomena see Chapter 12.

### 22.3 RADIO CHARACTERISTICS OF THE MOON AND PLANETS

In studies of the moon and planets two approaches are possible. One is passive: radio emission from the moon or planet is received and its spatial and radio-frequency spectral characteristics are analyzed. This passive approach is used to study the thermodynamic emission properties. Studies of the thermal component of the source permit investigation of the emissivity and thermal conductivity of the surface and subsurface, and of the thermodynamic and compositional properties of the atmosphere. Studies of the nonthermal component permit investigation of the origin, time variation, and precipitation of charged particles trapped in magnetic fields.

The other approach (radar) is active. Radio signals are beamed at the moon or planet and the temporal and Doppler-broadened bandwidth characteristics of the reflected energy are analyzed. Such studies permit investigation of planetary orbits, interplanetary distances, reflectivity, and rotation rates.

#### 22.3.1 Radio Emission of the Moon

Observations of radio emission from the moon are available in the wavelength range of 1.3 mm to 1.68 m. During lunation large measurable temperature changes are found at 1.3 mm to 3 cm, but no significant changes are observed at 20 cm or

longer wavelengths. Attempts to observe variations of lunar temperature during lunar eclipses reveal no significant changes in temperature at wavelengths greater than 1 cm. Observations at 4.3 mm showed a change from 232°K during the eclipse to 238°K one hour after the eclipse of August 25, 1961.

There are two components of the lunar radiation. The constant component,  $T_0$ , is the time average of the emission temperature over one lunation; there is no strong dependence on wavelength in this component. The variable component,  $T_1(\lambda)$ , shows strong dependence upon wavelength. It is as high as 25% of the constant component at millimeter wavelengths, but decreases with increasing wavelength.

The experimental dependence of temperature upon the lunar phase is approximated very well by

$$T_m(\lambda) = T_0 + T_1(\lambda) \cos [(2\pi t/P) - \xi(\lambda)] ; \quad (22-22)$$

$T_m(\lambda)$  is the measured radio-brightness temperature of the moon,  $t$  is the time of observation in the units of  $P$ ,  $P$  is the lunar synodic period (29.53 day), and  $2\pi t/P$  is the phase angle of the visible lunation measured from full moon. The phase lag,  $\xi(\lambda)$ , of the variable component is usually given in angular degrees ( $360^\circ$  is 29.53 day). (For substitution into Eq. (22-22), multiply angular degrees by  $1.745 \times 10^{-2}$  to obtain radians, or multiply radians by 57.2958 to obtain angular degrees.) The phase lag behind the visible lunar phase is small in the infrared and very short millimeter range. From the infrared to 1 cm the phase lag increases as the wavelength increases. At 1.25 cm the maximum brightness temperature occurs at  $45^\circ$  (about three and one-half days) after full moon. The phase lag does not appear to become greater than this at longer wavelengths. Because  $T_1$  decreases as  $\lambda$  increases it becomes difficult to measure the phase lag at longer wavelengths. For  $\lambda > 20$  cm,  $T_1$  cannot be measured, so phase lag becomes indeterminate.

The lunar surface is partially transparent to radio waves. From the wavelength dependence and phase lag of the variable component, it is deduced that the longer wavelength emission comes not from the lunar surface but from a region somewhat below the surface; the longer the wavelength, the greater the depth below the surface at which the radiation originates.

Table 22-1 gives some of the experimental values of  $T_0$ ,  $T_1$ , and  $\xi$  at different wavelengths. These observations by various radio astronomers indicate that the time average of the lunar radio brightness (the constant component) at the center of the lunar disk is about 215°K. For a description of accurate lunar radiometric measurements see Troitsky [1965].

Table 22-1. Experimental Brightness-Temperature Parameters of the Moon

Wavelength (cm)	Temperature* (°K)		Phase Lag (deg)	Estimated Error (%)
	T <sub>0</sub>	T <sub>1</sub> (λ)		
0.13	219	120	16	15
0.40	204	56	23	4
0.80	211	40	30	15
1.25	215	36	45	10
1.63	208	37	30	3
3.15	195	12	44	15
3.2	210	13	55	2.5
3.2	213	14	26	2
9.6	218	7	40	2.5
14.2	221	—	—	3.5
32.3	233	—	—	2.5
70	217	—	—	8
168	233	—	—	4

\*T<sub>0</sub> is the constant component, and T<sub>1</sub>(λ) the variable component during lunation.

### 22.3.2 Radio Emission of the Planets

Assuming that the major source of heating is solar radiation, the temperature at the subsolar point (sun at zenith of point) of a smooth nonrotating sphere having low heat conductivity (and no atmosphere) would be

$$T_{SS} = 392(1 - \alpha)^{1/4} R^{1/2} \text{ [°K] } , \quad (22-23)$$

where  $R$  is the distance to the sun in astronomical units and  $\alpha$ , the Bond albedo, is defined as the ratio of the total flux reflected in all directions to the total incident flux. The mean or effective temperature,  $\bar{T}$ , would be  $0.84 T_{SS}$  for the illuminated hemisphere and zero for the dark hemisphere.

If a planet is rapidly rotating, or the thermal conductivity is large, or there is an appreciable atmosphere that distributes the heat received over the entire surface, the mean temperature will be the same for both hemispheres. This effective temperature is

$$\bar{T} = 277(1 - \alpha)^{1/4} R^{1/2} \text{ [}^\circ\text{K]} \quad (22-24)$$

The antenna temperature contribution received from a planet is

$$T_A = \epsilon \bar{T} \Omega_s / \Omega_A = \epsilon \bar{T} \Omega_s A_e / \lambda^2 \quad (22-25)$$

where  $\Omega_s$  is the solid angle of the planet as viewed from the radio telescope, and  $\epsilon$  is the emissivity of the planet. It is assumed in Eq. (22-25) that  $\Omega_s \ll \Omega_A$ , obviously true for planets but not usually true for the moon. The emissivity,  $\epsilon$ , may be determined from radar measurements of the planetary reflectivity,  $r$ ;

$$\epsilon = 1 - r \quad (22-26)$$

When  $r$  cannot be measured,  $\epsilon$  can be assumed to lie within the range 0.9 to 1. It is usual to define a disk brightness temperature,  $T_b \equiv \epsilon \bar{T}$ ;  $T_b$  is thus the equivalent blackbody temperature of a planet subtending a solid angle  $\Omega_s$  that would give the observed antenna temperature, or the flux density [Eq. (22-6)].

Infrared measurements are usually made with bolometers, which respond to the total radiant flux received from the planet. This total flux (radiant emittance) is proportional to the fourth power of the temperature [Eq. (B-7)], so that values of mean temperature obtained by such observations are heavily weighted by the hotter regions. The flux density measured over a narrow bandwidth at radio frequencies is directly proportional to the temperature, Eq. (22-6) or Eq. (22-7). The contribution of the lower temperature regions of a planetary body are therefore brought out more fully by radio-frequency measurements at narrow bandwidths.

Table 22-2 is a summary of the planetary temperatures observed at various wavelengths; for detailed accounts see Mayer [1964] or Kellerman [1966]. Radio emissions from Neptune and Pluto have not been detected.

22.3.2.1 Mercury. Observations of radio emission from Mercury show a mean temperature of  $400 \pm 160^\circ\text{K}$ .

22.3.2.2 Venus. Measurements show that at centimeter wavelengths the equivalent disk temperature is about  $600^\circ\text{K}$ . Because the atmosphere of Venus should be relatively transparent to wavelengths of 3 cm or greater (little absorption by atmospheric gases), the radiation at these wavelengths is assumed to originate at or near the planetary surface. There is some evidence [Drake, 1964; Kellerman, 1966] that at  $\lambda < 20$  cm the emission temperature decreases to around 500 to  $530^\circ\text{K}$ , but the signal-to-noise ratio is so poor at these frequencies that this result is doubtful. At millimeter wavelengths the observed temperatures decrease to about 300 or  $400^\circ\text{K}$  [Tolbert and Straiton, 1964]. The atmospheric gases have a much higher absorption

Table 22-2. Equivalent Blackbody Temperatures of Planets

Wavelength (cm)	Temperature (°K)					
	Mercury	Venus	Mars	Jupiter	Saturn	Uranus
21	---	590	225	---	303	---
11	---	629	191	---	196	130
10	---	660 b 580 d	209	---	---	---
6	---	---	226	---	179	---
3	400	690 b 550 d	211	140	106	---
0.86	---	375 400	230	113	116	---
0.43	---	330	---	105	103	---
0.32	---	300	240	111	97	---

b. Observations on bright side.

d. Observations on dark side.

at millimeter wavelengths; therefore, this radiation may originate at higher levels in the atmosphere where the emission (equivalent blackbody) temperature is that much lower.

22.3.2.3 Mars. Measurements at various wavelengths by many observers indicate that Mars has an equivalent blackbody temperature of about 225°K; this agrees closely with infrared observations. Because the temperatures are roughly the same at centimeter and millimeter wavelengths, the atmosphere of Mars is not highly absorbing. There is no indication of any nonthermal emission.

22.3.2.4 Jupiter. The apparent blackbody temperature increases with wavelength from about 140°K at 3 cm to 50,000°K at 68 cm. There are also indications of long-time changes in radio emission. Some, but not all, observations indicate changes in emission as a function of rotation. At 31 cm the radiation is about 30% linearly polarized with the electric vector approximately parallel to Jupiter's equator. The source of polarization seems to be an equatorial ring about three times the diameter of Jupiter. In general, there are three different kinds of radio emission from Jupiter, thermal radiation and two types of nonthermal radiation. Measurements at millimeter wavelengths [ Tolbert, 1966] indicate that the thermal component of Jupiter's emission temperature is roughly 110°K. At very short centimeter wavelengths emission is predominantly thermal radiation from the disk. At decimeter

wavelengths the predominant source is nonthermal and may be radiation from charged particles with relativistic energies that are trapped in Jupiter's magnetic field. The polarization of the 31-cm radiation from Jupiter lends support to this theory. At very long wavelengths (near 15 m) the nonthermal emissions are short intense bursts that have extensive fine structure; these events are strongly influenced by the position of Jupiter's satellite Io.

22.3.2.5 Saturn. Measurements at millimeter wavelengths indicate that the equivalent blackbody temperature of the thermal emission of Saturn is roughly 105°K, in good agreement with the infrared temperature determinations. Measurements at wavelengths greater than 3 cm indicate that the apparent blackbody temperature increases with increasing wavelength. The increase in temperature toward the longer wavelengths might be due to the presence of a nonthermal component such as occurs in the centimeter radiation from Jupiter.

22.3.2.6 Uranus. Measurements at 11.3 cm give an equivalent blackbody temperature of  $130^\circ \pm 40^\circ\text{K}$ . At 3.75 cm a temperature of  $159^\circ \pm 16^\circ\text{K}$  is obtained.

### 22.3.3 Radar Observations of the Moon

Radar observations of the moon provide: (1) very accurate range measurements; (2) the specific reflectivity or relative cross section at various wavelengths; (3) the angular dependence of scattering by the lunar surface; and (4) deduced values of the dielectric constant. Investigations have been made at wavelengths from 8.6 mm to 19.2 m; for a summary see Evans [1965].

Recent measurements reported by the Naval Research Laboratory give a value of  $384,400.2 \pm 1.1$  km for the mean center-to-center distance between the Earth and the Moon. The calculation is based on a value of 6,378.17 km for the Earth's radius, which is most consistent with the observed diurnal variation in range.

Radar reflectivity of a planetary body is usually expressed as a relative cross section  $\sigma/\pi a^2$ , where  $\sigma$  is the absolute scattering cross section and  $a$  is the planetary radius. Table 22-3 lists experimentally determined values of the relative radar cross section of the Moon at various wavelengths. The results suggest that the cross section remains constant at about 7% of the projected area of the lunar disk for wavelengths in the range of 1 cm to 1 m, and perhaps rises to 10% or more at longer wavelengths.

The angle of incidence of the radar signal on the lunar surface varies from zero at the center of the lunar disk to  $90^\circ$  at the edges. The projected area presented to the incident radar signal varies as the cosine of the incidence angle. Short pulse observations are used to explore the angular dependence of radio-wave scattering by the lunar surface. One component of the echo arises from the highlight located

Table 22-3. Relative Radar Cross Sections of the Moon

Wavelength (cm)	Relative Cross Section ( $\sigma/\pi a^2$ ) <sup>*</sup>
0.86	0.07
3.0	0.07
3.6	0.07
10.0	0.07
33.5	0.09
73.0	0.074
100	0.07
150	0.08
300	0.10
1130	0.19
1560	0.13
1920	0.16

\*  $\pi a^2$ , the physical cross section (area of the lunar disk) is  $9.49 \times 10^{12} \text{ m}^2$ .

at the center of the lunar disk; a second component comes almost equally from the remaining parts of the surface. Figure 22-2 shows that the division of return power between the two components changes markedly with wavelength. At 8.6 mm only 15% of the return power is from the highlight, but at 68 cm roughly 80% of the power returned is from the highlight.

Deduced values of the dielectric constant range from 2.79 at 68 cm, to 2.72 at 3.6 cm. These values indicate that the lunar surface is broken or porous in texture.

#### 22.3.4 Radar Observations of the Planets

Radar has been used to investigate Mercury, Venus, Mars, and Jupiter. For Mercury there is agreement among several observers that the relative radar cross section is roughly 0.06, similar to the value for the moon. Measurements by Pettengill and Dyce [1965] show the rotation period of Mercury as  $59 \pm 5$  days; previously it was believed to be synchronous with the 88-day orbital period.

Venus has a relative radar cross section between 0.1 and 0.2; the higher values are generally associated with observations at the longer wavelengths. Two different measurements of the rotation period of Venus agree closely; one is  $250 (+4, -7)$  days, the other is  $247 \pm 5$  days. The rotation is retrograde, that is, opposite to the sense of rotation of the earth. For a discussion of the radar observations of Venus see Carpenter [1966].

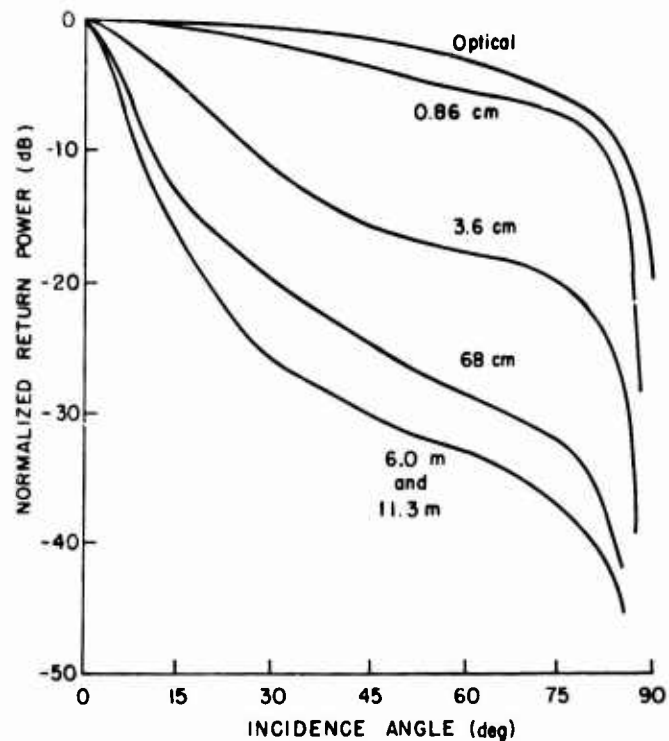


Figure 22-2. Relative return-power from the lunar surface as a function of the angle of incidence of the radar signal; power normalized at zero-degree incidence,  $P(0^\circ) \equiv 1$ . Wavelength of the signal is given below each curve.

The relative radar cross section of Mars is in the range 0.03 to 0.09 with large fluctuation according to the face of the planet presented to the radar signal. Mars appears smoother than other planets with a marked degree of surface variation.

From the size of and the distance to the planet, Jupiter should be a reasonable target for present-day radars, but Jupiter is an exceedingly poor reflector of radio energy. Various reports of reflections detected from Jupiter have not yet presented evidence that could be confirmed. Measurements at 70 cm set an upper limit on the specific reflectivity at 0.00045. It is possible that measurements at other wavelengths will yield significantly different results.

## 22.4 MAPS OF BACKGROUND RADIATION

Many surveys of the background radio emission at various frequencies are available. All surveys show that most of the radio-emission background is due to radiation from the galactic plane. Radio emission increases toward the galactic center and is minimum near the galactic poles.

Figures 22-3 through 22-7 are contour maps compiled from observations at 38, 81, 250, 400, and 960 MHz, plotted in equatorial coordinates ( $\alpha$ , right ascension and  $\delta$ , declination). Observations made with a particular radio telescope may not agree exactly with these maps because of differences in antenna size and shape, receiver sensitivity, and values of absolute calibration.

## 22.5 DISCRETE SOURCES OF RADIO EMISSION

In addition to the background radio radiation, there are certain small areas that emit additional radiation; these are called discrete radio sources. Each source subtends a small solid angle it is sometimes called a localized source. A point source is an idealization of a localized source; it may be defined as one that subtends an infinitesimal solid angle. An extended source is a discrete source of relatively large angular extent. The dividing line between localized and extended sources is arbitrary; the usual practice is to regard sources with angular diameters greater than one degree as extended sources.

One of the distinguishing characteristics of a discrete radio source is that the flux density depends on the wavelength. This variation with wavelength is proportional to  $\lambda^n$ ;  $n$  is the spectral index of the radio source.

If the temperature of a radio source is constant with wavelength,  $n = -2$  and the source is called a thermal source. Sources for which the temperature is not constant with wavelength ( $n \neq -2$ ) are called nonthermal sources. Nonthermal radiation caused by emission from relativistic electrons moving in weak interstellar magnetic fields is called synchrotron emission. Most discrete radio sources are nonthermal and their flux density increases with increasing wavelength ( $n > 0$ ).

### 22.5.1 Flux Densities and Spectra

Most measurements of discrete radio sources have been made at one or two frequencies by observers using distinctively different types of antennas and radiometers. Numerous lists or catalogues of the flux densities of radio sources at particular frequencies are available; for example see Howard and Maran [1965]. In the region 10 m to 30 cm, a comprehensive reference on the spectra of many radio sources is Conway, Kellermann, and Long [1963].

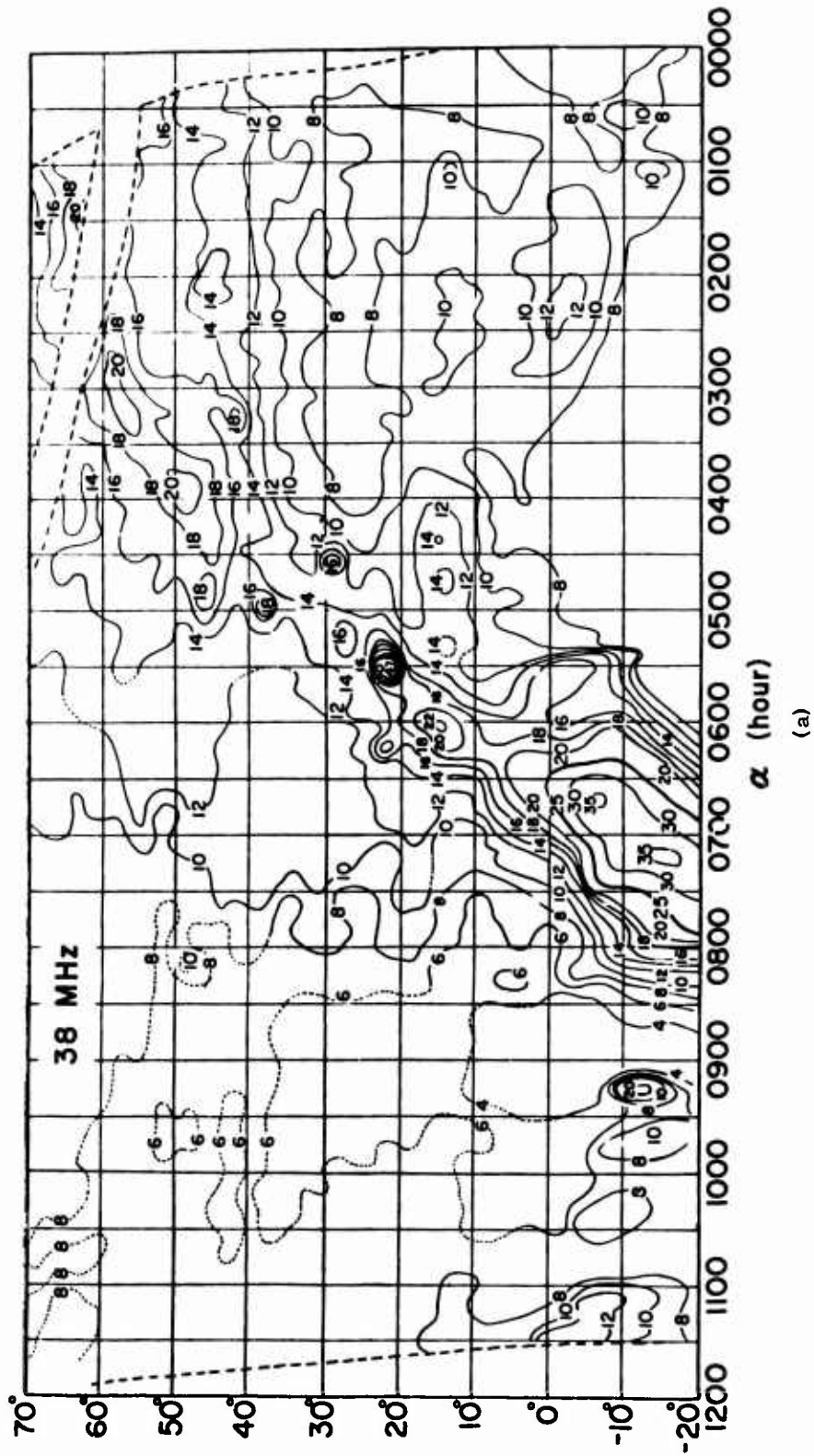
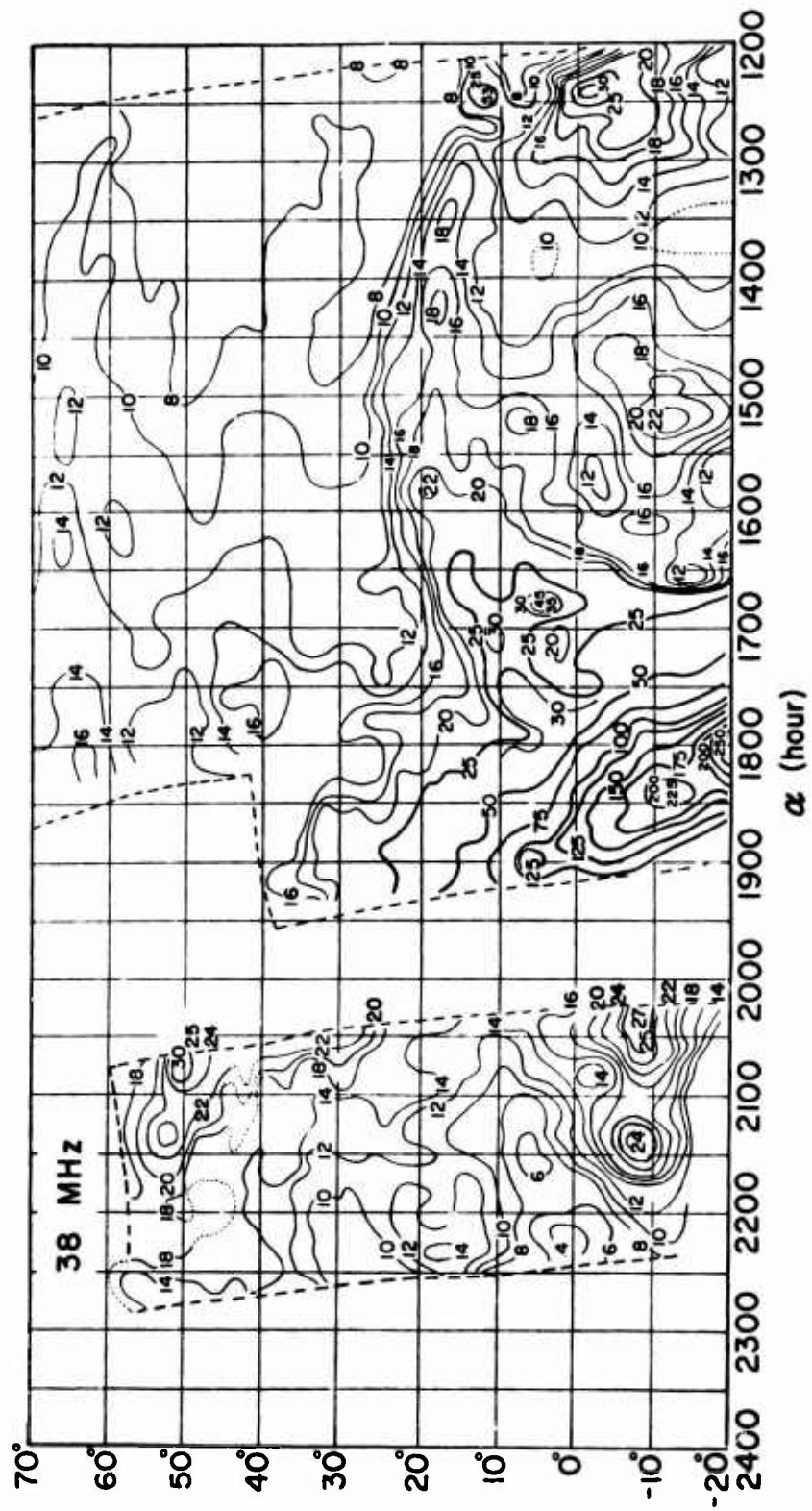


Figure 22-3. Galactic radio emission at 38 MHz. Each contour represents 1000°K. (From J.H. Blythe, Monthly Notices Roy. Astron. Soc., v. 117, no. 6, p. 652, 1957.)



(b)

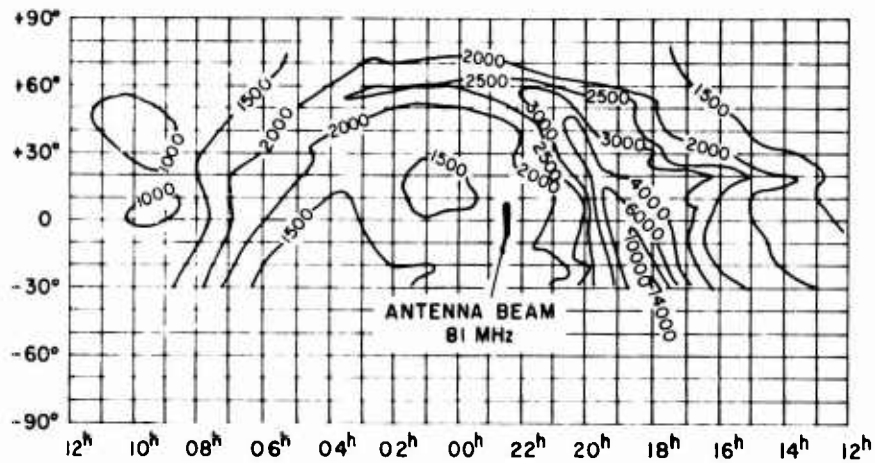


Figure 22-4. Background radiation at 81 MHz. Contour units are °K. (After H.C. Ko, Proc. IRE, v.46, no.1, p.208, 1958).

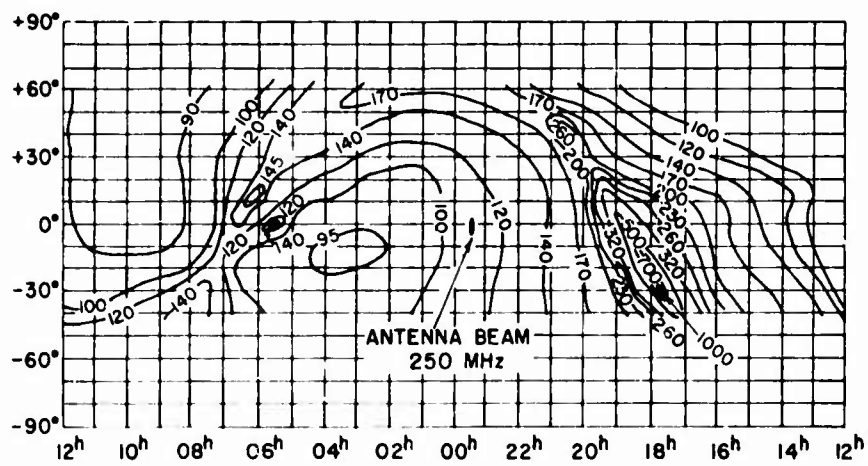


Figure 22-5. Background radiation at 250 MHz. Contour units are °K. (After H.C. Ko, Proc. IRE, v.46, no.1, p.208, 1958).

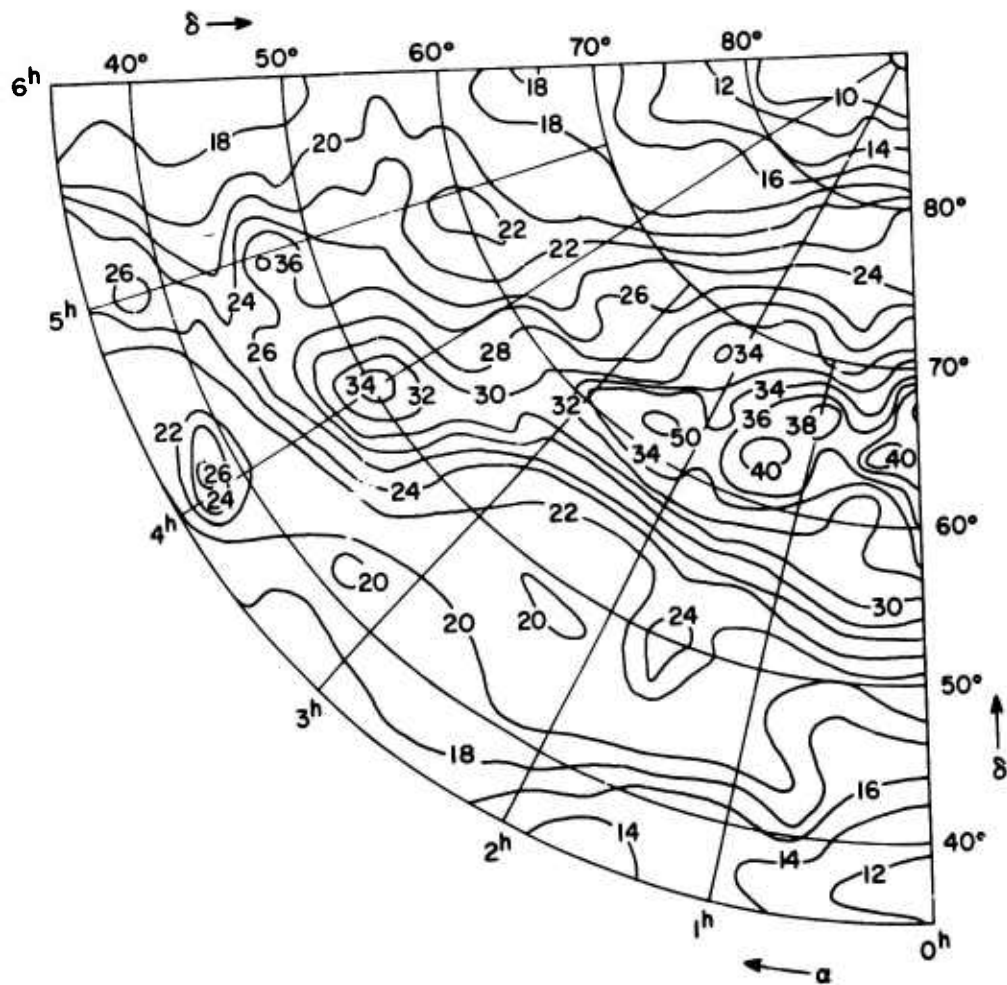


Figure 22-6a

Figure 22-6 (a through j). Background radiation at 400 MHz. To obtain brightness temperatures ( $^{\circ}\text{K}$ ) from the contour units, use the relation  $T_b = 0.9 (\text{units} + 14)$  [Seeger et al., 1965]

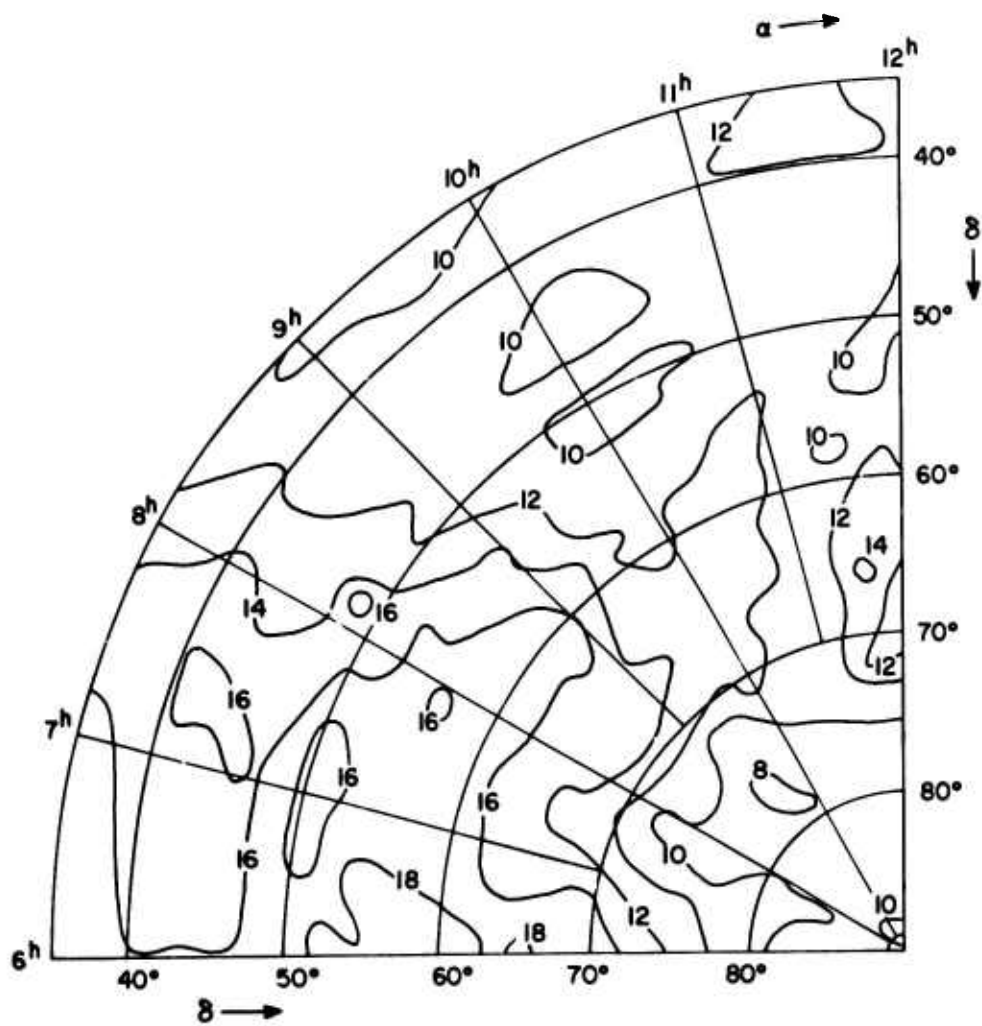


Figure 22-6b

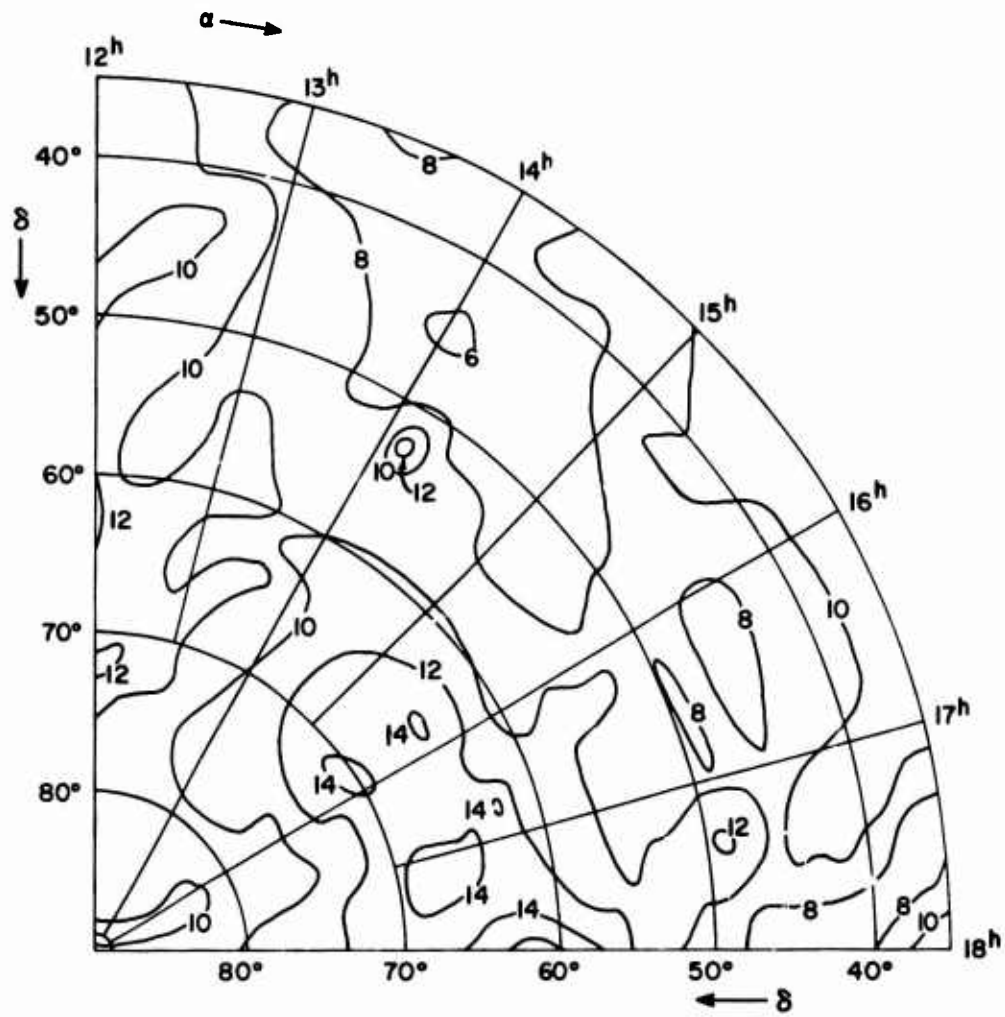


Figure 22-6c

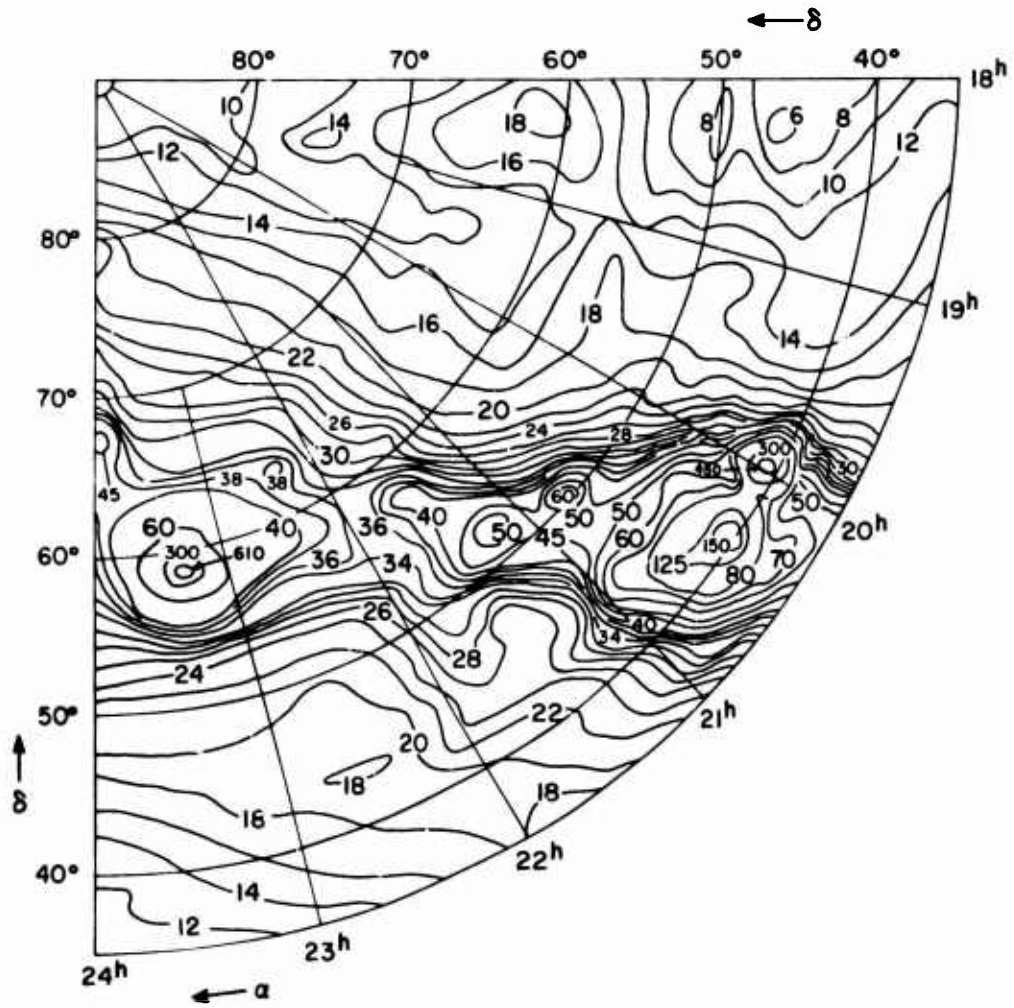


Figure 22-6d

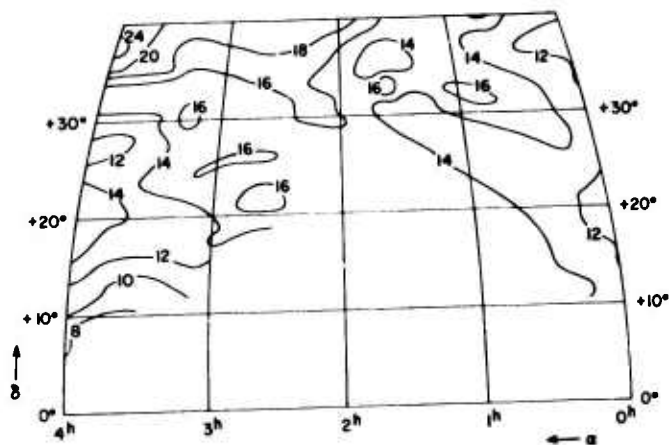


Figure 22-6e

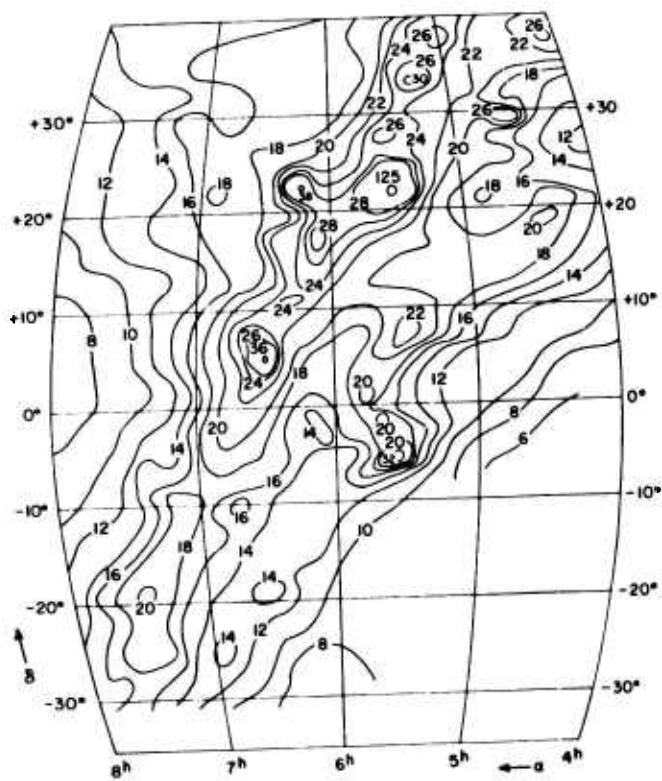


Figure 22-6f

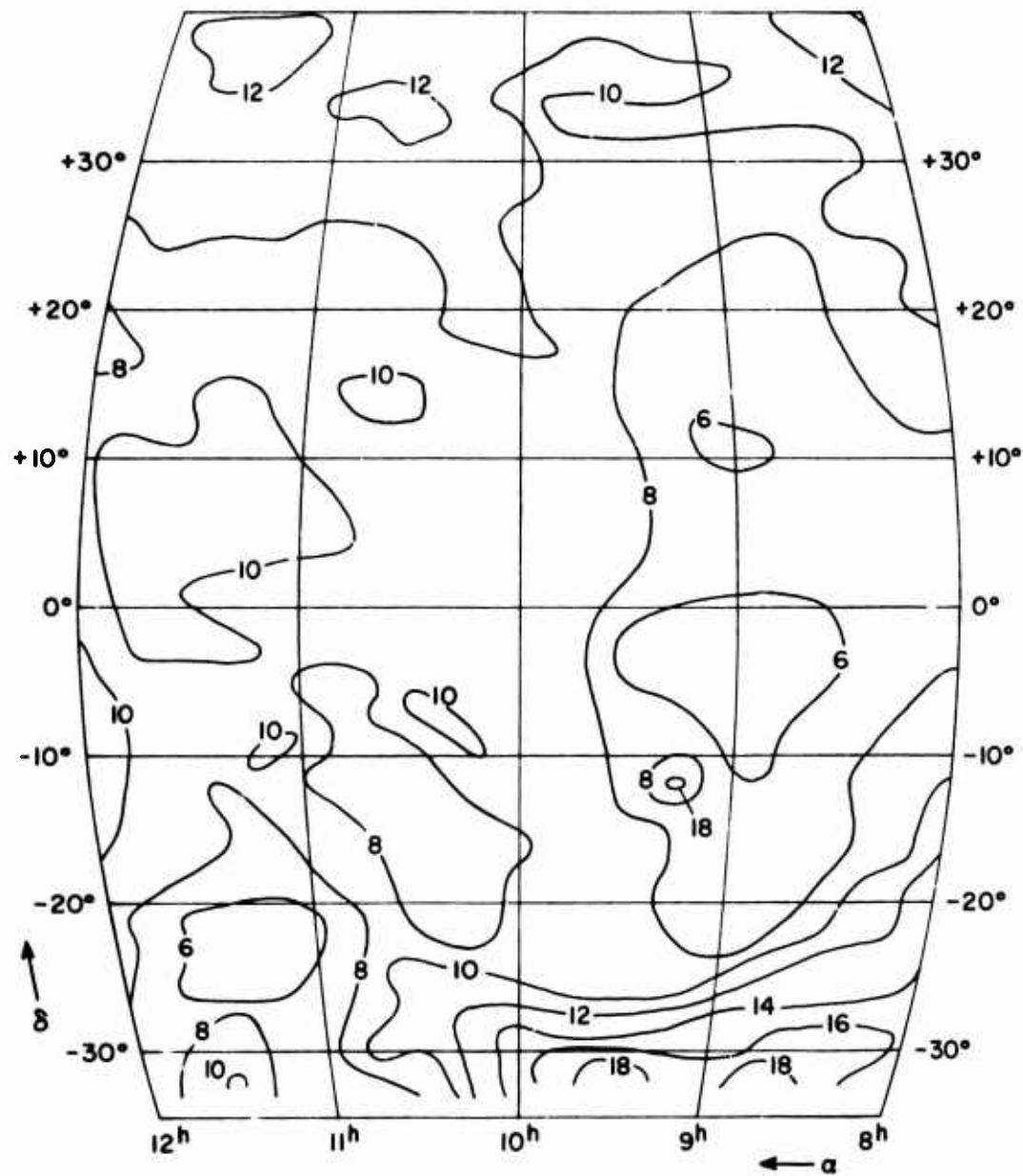


Figure 22-6g

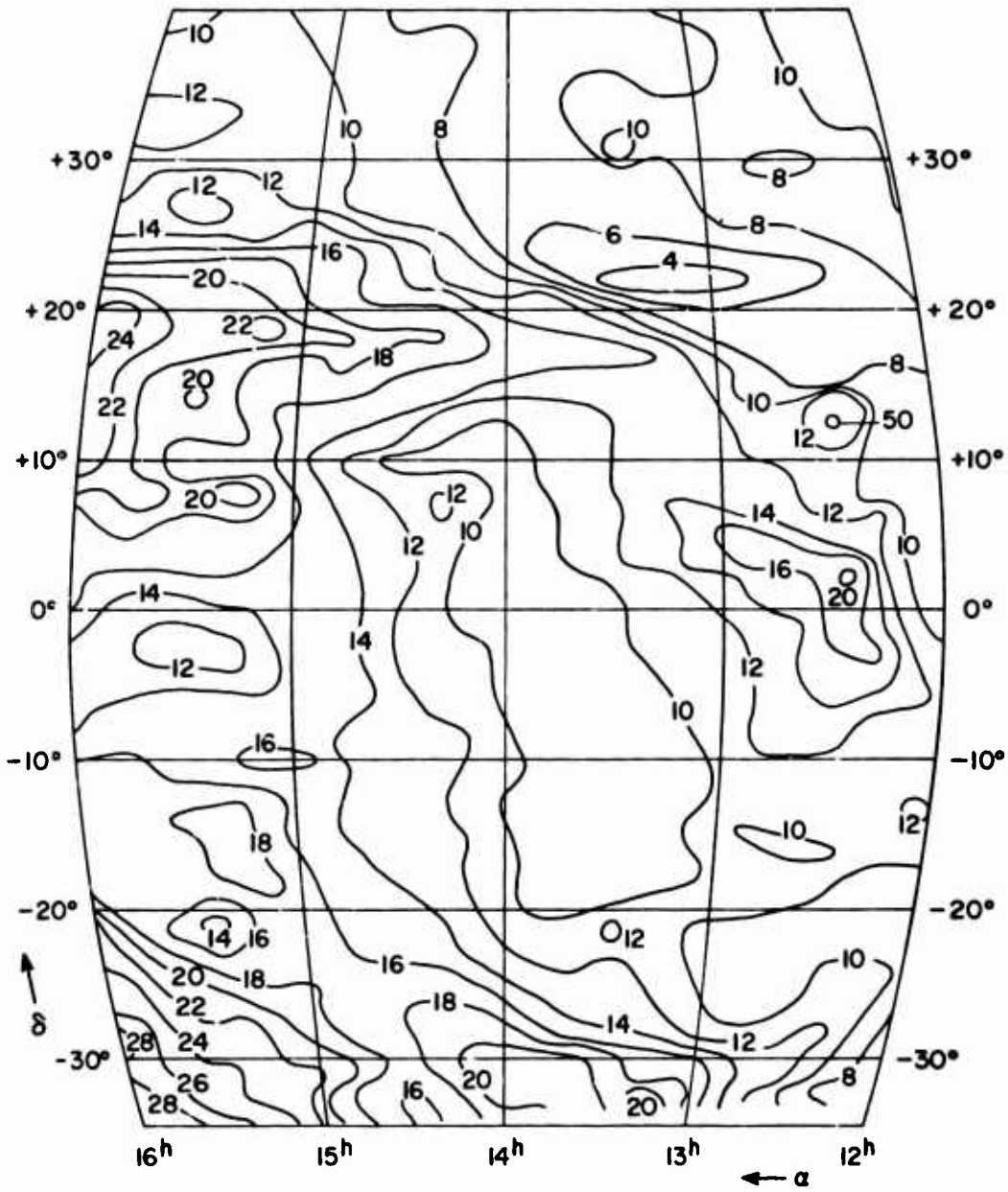


Figure 22-6h

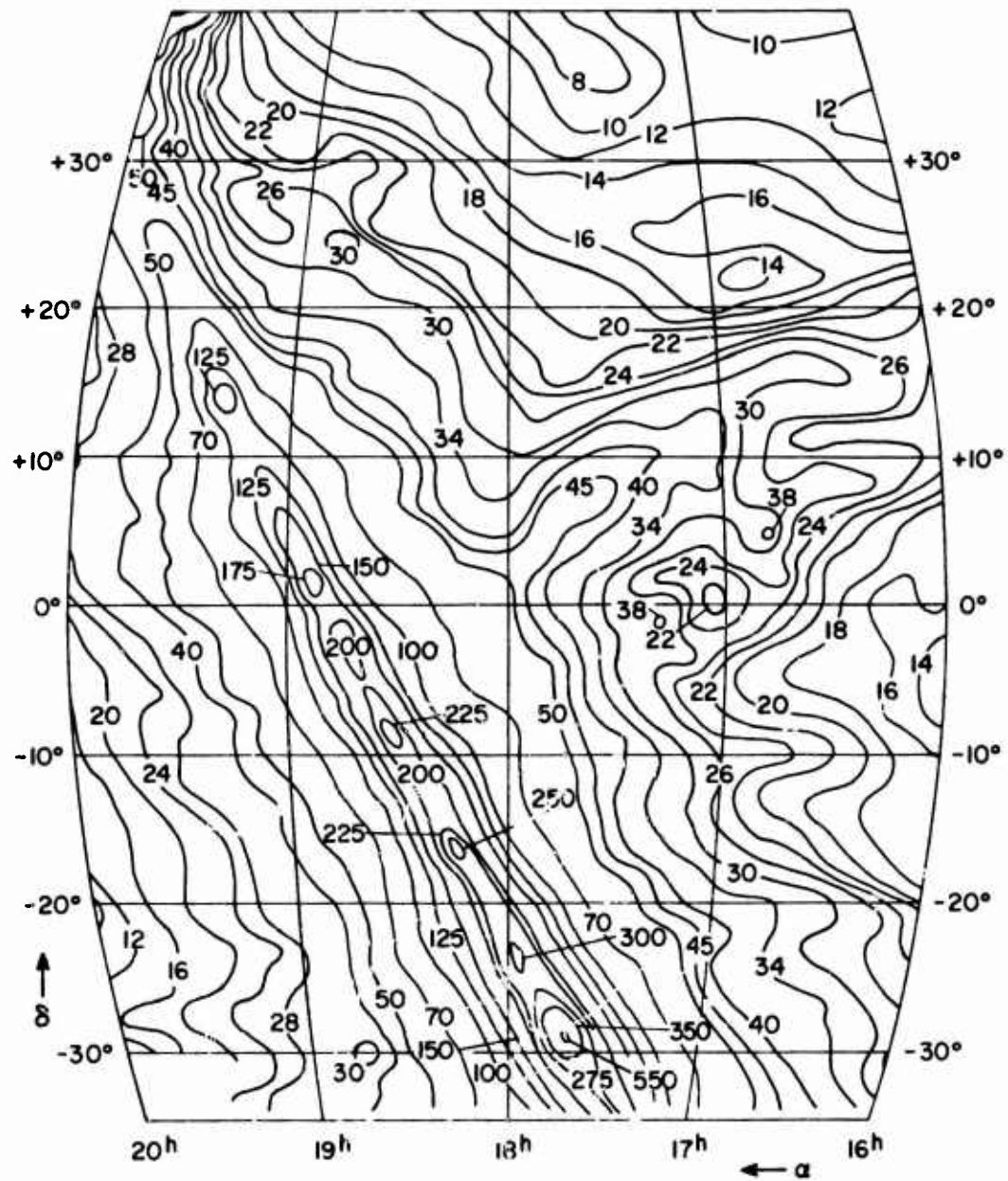


Figure 22-6i

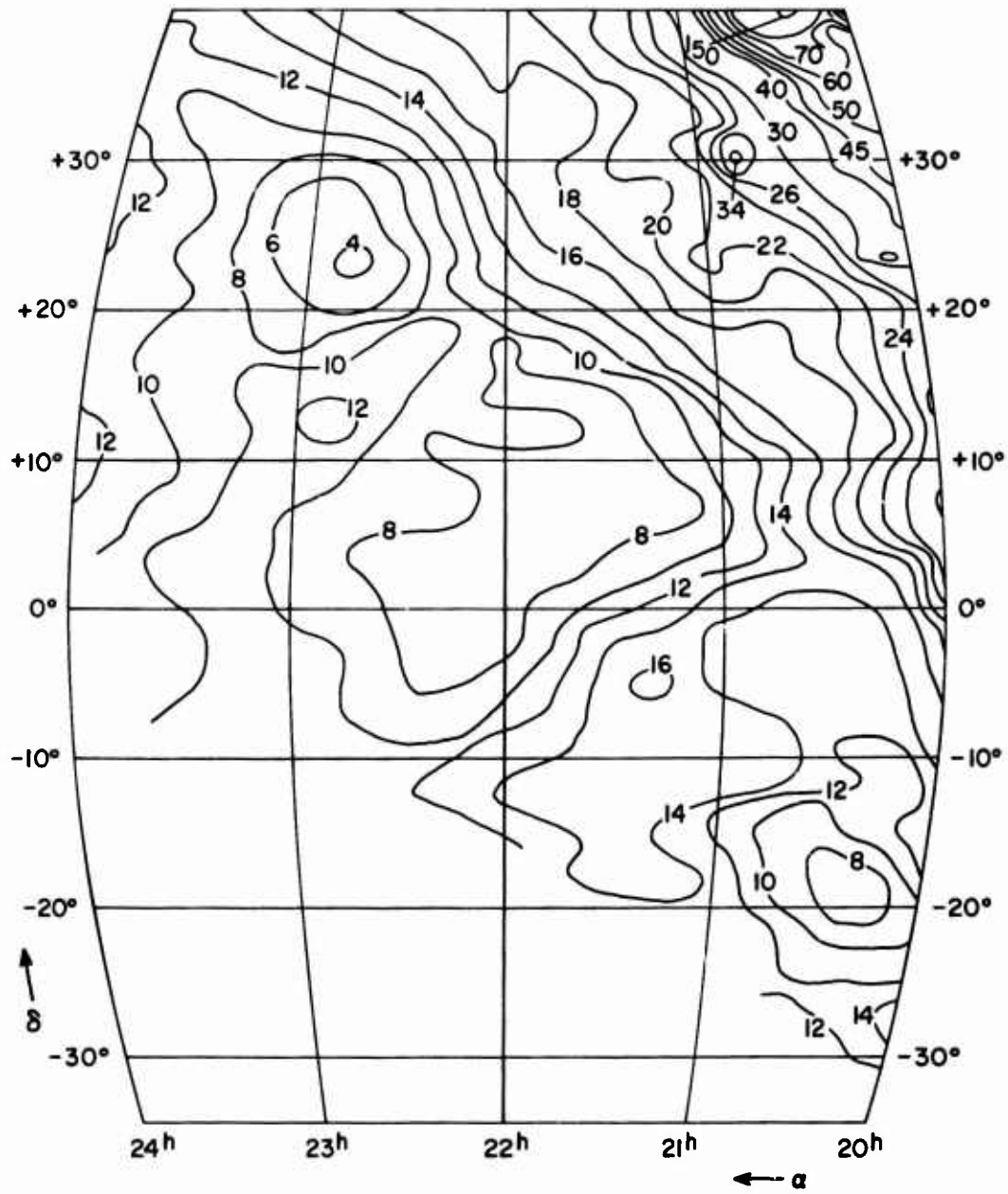


Figure 22-6j

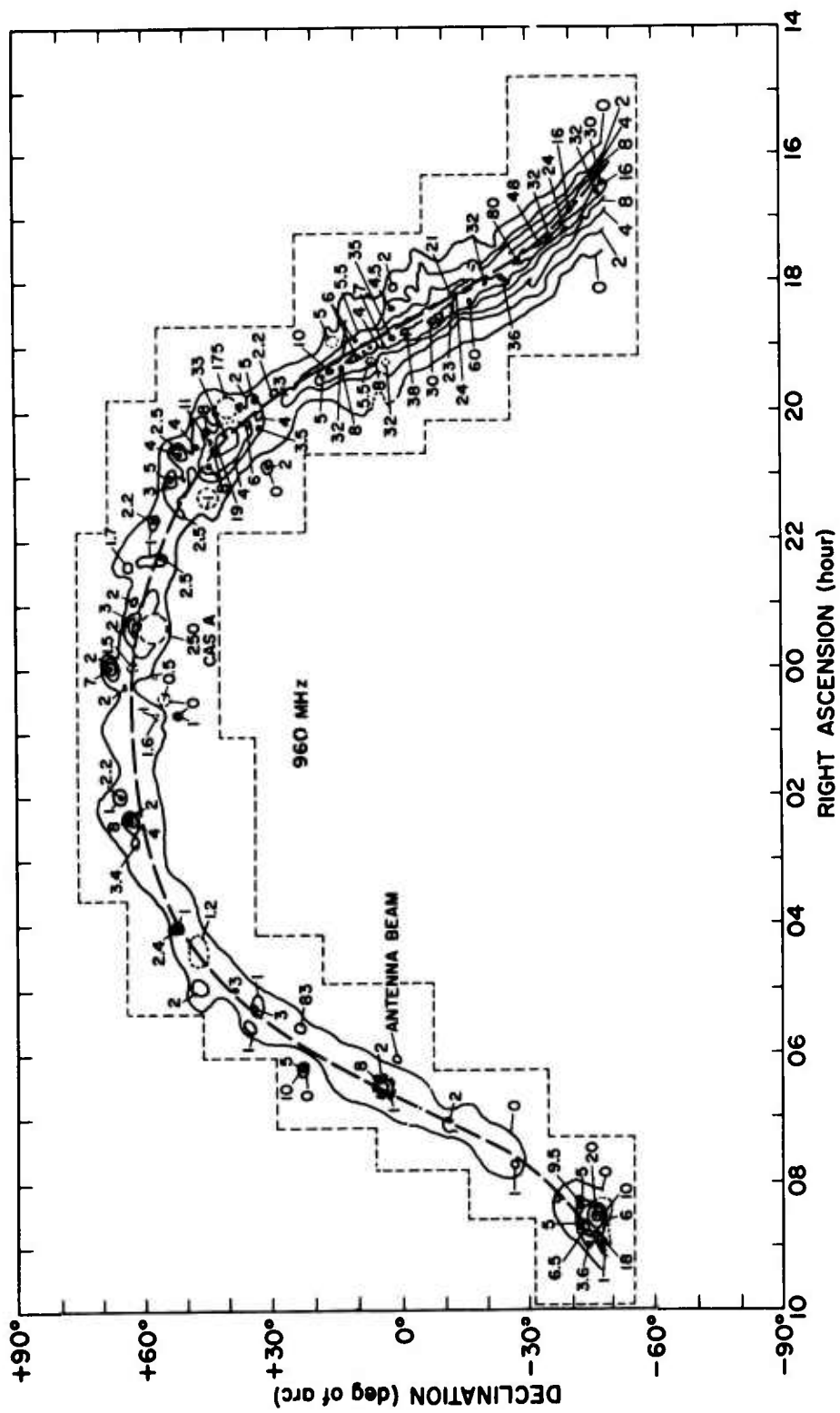


Figure 22-7. Background radiation at 960 MHz. The contours represent steps of 1.25°K in observed antenna temperature above an arbitrary-zero baseline. (From R. W. Wilson and J. A. Bolton, Publ. Astron. Soc. Pacific, v. 72, no. 428, p. 331, 1960.)

At long wavelengths it becomes increasingly difficult to determine the spectra of radio sources. Variable ionospheric absorption and the presence of interfering radio stations limit the times of day during which observations are feasible. With increasing wavelength the flux density (and thus the antenna temperature due to the source) increases according to  $S \propto T_A \propto \lambda^n$ , with  $n$  generally in the range zero to one. However, the antenna temperature due to the background increases at a much greater rate,  $T_A \propto T_{\text{sky}} \propto \lambda^{2.5}$ . Extremely large apertures or very long baselines are needed to obtain adequate resolution for discrimination of the source against this background. However, spectral characteristics at dekameter wavelengths are known for some radio sources [Guidice, 1966; Erickson and Cronyn, 1965].

Figure 22-8 shows the spectra, in the region from about 20 m to 3 cm, of the five brightest discrete sources; Cassiopeia A, Cygnus A, Taurus A, Virgo A, and Centaurus A. Table 22-4 gives their positions (the equatorial coordinate system) and their angular diameters. Table 22-5 lists their flux densities at various frequencies; note that the flux density of Cassiopeia A decreases roughly one percent per year.

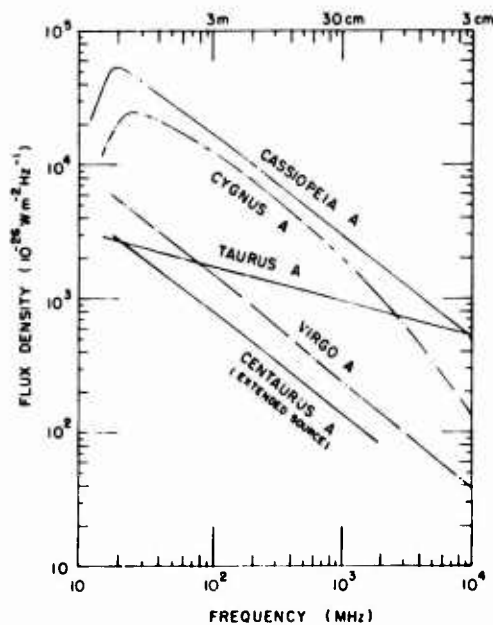


Figure 22-8. The spectra of the five strongest radio sources; values for Cassiopeia A (a variable source) are for the year 1964.

In the centimeter and meter wavelength regions the value of the spectral index of most radio sources is in the range 0.2 to 1.0. Most nonthermal sources have a spectral index that is roughly constant in this wavelength region. There are important exceptions, however. As Figure 22-8 shows, the very strong radio source Cygnus A has a curved spectrum in this region.

Figure 22-9 illustrates the various shapes of the spectral curves of different types of discrete radio sources. Sources with very high surface-brightness temperature (for example sources of moderate flux density but with extremely small angular diameter) have spectra that flatten out or curve downward at dekameter wavelengths. Quasi-stellar radio sources (quasars) such as 3C 48, have this type of spectrum. The leveling-off, or decrease, of flux density with increasing wavelength is caused by synchrotron self-absorption.

Table 22-4. Positions and Angular Diameters of the Brightest Discrete Radio Sources

Source	Right Ascension*			Declination*		Angular Diameter (min)	Comments
	h	m	s	(deg)	(min)		
Cassiopeia A	23	21	11	58	32.8	3.8	Circularly symmetrical. Flux density decreases about 1% per year
Cygnus A	19	57	44.4	40	37.4	<0.7 each	Two sources, intensity ratio 1.2:1, separation 1.58 min on axis at 109°
Taurus A	05	32	31	21	59.0	3.5	Radiation concentrated in inner mass of Crab Nebula
Virgo A	12	28	16.9	12	39.9	0.6 core 6.5 halo	Halo contributes 55% of the flux density at 400 MHz and almost all the flux density below 50 MHz
Centaurus A	13	22	36	-42	48.4	3.8 2.0	Two sources, approx. equal intensities, separation of 7.1 min on axis at 46°. Extended source covers a region 3° by 8°

\*Coordinates for epoch 1950.0 [Howard and Maran, 1965].

Table 22-5. Flux Densities of the Brightest Discrete Radio Sources

Frequency (MHz)	Flux Density ( $10^{-26} \text{ W m}^{-2} \text{ Hz}^{-1}$ )				
	Cass A*	Cygnus A	Taurus A	Virgo A	Cent A**
20	54,000	20,000	2,700	5,400	2,800
40	34,000	21,000	2,250	3,100	1,600
70	22,600	15,500	1,950	2,000	1,050
100	17,300	12,000	1,750	1,500	800
200	10,300	7,500	1,480	860	470
400	6,100	4,400	1,220	500	280
800	3,700	2,600	1,040	320	180
1,500	2,300	1,400	880	180	100
3,000	1,380	670	730	100	---
6,000	820	290	610	58	---
10,000	500	150	530	38	---

\* Flux density decreases approximately 1% per year; values given are for 1964.

\*\* Flux densities given are for the extended source.

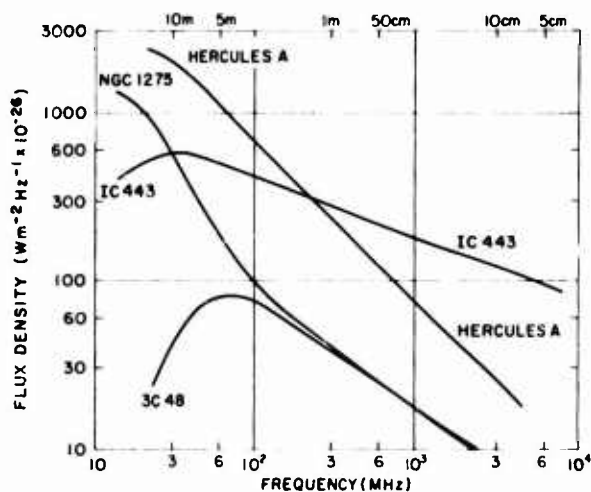


Figure 22-3. The spectra of various types of discrete radio sources

Radio sources associated with double or elliptical galaxies (for example, Hercules A and Cygnus A) have spectra that gradually level off with increasing wavelength and eventually curve downward at the longer wavelengths. This spectral characteristic is also found in some sources that are remnants of supernovae (for example, Cassiopeia A and IC 443). The flattening of these spectra at dekameter wavelengths is probably caused by absorption in HII regions.

Core-and-halo sources [for example, Virgo A and NGC 1275 (Perseus A)] consist of a small dense central core surrounded by an ionized medium (the halo) that is much less dense. Their spectra curve upward with increasing wavelength in the dekameter region; this curvature may be slight or quite prominent. (For the source NGC 1275 the observed flux density at 22 MHz is more than three times the value that would be obtained if its spectrum from 3000 to 178 MHz were extrapolated to 22 MHz.) This effect, called halo predominance, is characteristic of core-and-halo sources. Because the spectral index of the halo is larger than that of the core, as the wavelength increases the contribution of halo radiation to the observed flux also increases. At meter wavelengths the radiation from the core exerts a significant influence on the shape of the spectrum. At dekameter wavelengths the radiation of the halo predominates; the slope of the spectrum approaches asymptotically the spectral index of the halo.

#### 22.5.2 Sources With Large Variations in Flux Density

Observations over a period of several years show variations the order of 50% in the flux densities at 3.75 and 1.8 cm of some radio sources. For example, at 3.75-cm wavelength the flux density of NGC 1275 more than doubled in about six years [Dent, 1966].

Figure 22-10 illustrates the shape of the spectral curves of three variable sources; two are quasi-stellar sources (3C 273 and 3C 279) and one is the unusual Seyfert galaxy (NGC 1275). The spectrum of Virgo A is shown as a referent. The variable sources have flat spectra between 1 and 4 cm; this is characteristic of young, highly active sources in which large outbursts are still occurring. Sources

3C 279 and NGC 1275 show a sharp increase in flux density to their values at 1 to 4 cm. In contrast, it is characteristic of nonvarying sources (such as Virgo A) to have spectra that continue to decrease at wavelengths shorter than 4 cm. For wavelengths longer than 10 cm the flux densities of the variable sources decrease with decreasing wavelength. Theory indicates that this steep portion (longer wavelength) is probably due to radiation from the remnants of much earlier outbursts in these sources.

## 22.6 SPECTRAL LINE RADIATION

In contrast to the continuum radiation from extended regions and discrete sources, spectral line radiation is a resonant process resulting from transitions between energy levels of the emitting (or absorbing) atom or molecule. Therefore, detectors for spectral line work must be narrow band (as small as kHz for high resolution work), use either frequency sweeping or a large bank of narrow-band filters to cover the frequency range of interest, and have a very stable oscillator to determine and maintain exact frequency operation.

Observations of spectral lines are used to determine the large-scale structure of our Galaxy, such as concentrations of interstellar gas and clouds, the delineation of the spiral arms, rotational velocities about the galactic center, and velocities of interstellar clouds. Velocities of approach or recession along the line of sight are calculated from observations of the line broadening and of the Doppler shift in frequency. Regions (or clouds) which are predominantly neutral atomic hydrogen are called HI regions; the mean kinetic temperature of these regions is estimated to be about 125°K. HII regions surround extremely hot and luminous stars; in these regions, which have kinetic temperatures the order of  $10^4$  °K, practically all the

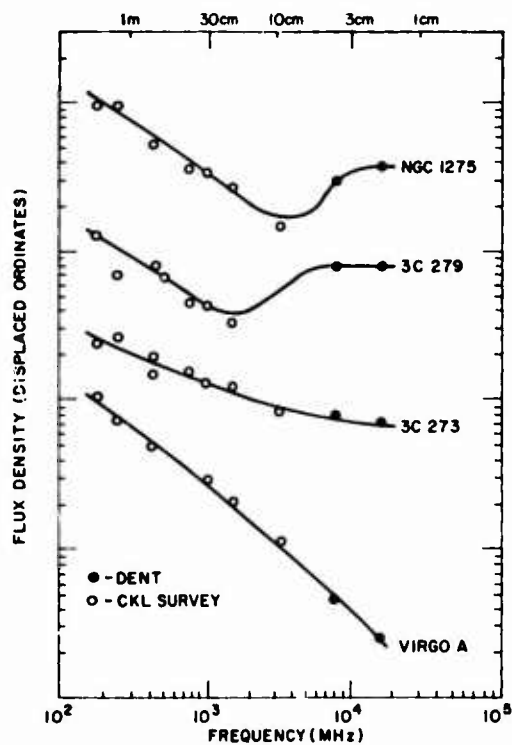


Figure 22-10. Shape of the spectrum of three variable radio sources (year 1964) compared with that of the normal non-thermal source Virgo A. Each curve is arbitrarily displaced on the ordinate scale; i. e., at 16,500 MHz, the observed flux of Virgo A is the same order of magnitude as NGC 1275 for the year 1964. (From W. A. Dent and F. T. Haddock, *Nature*, v. 205, p. 487, 1965)

hydrogen is ionized. For a review of studies of the interstellar gas and clouds see Dieter and Goss [1966].

Emission and absorption lines of atomic hydrogen and hydroxyl are described in the following sections. At present, helium is the only additional element detected by line radiation at radio frequencies. Emission lines of highly excited neutral helium were discovered in the Omega nebulae [Lilly, et al., 1966].

#### 22.6.1 The 21-cm Atomic Hydrogen Line

The line at the 21-cm wavelength results from the transition between the two hyperfine levels of the ground state of the neutral hydrogen atom; the rest-frequency of this line is 1420.4056 MHz. Because the energy difference between the levels is so small ( $5.6 \times 10^{-6}$  eV), excitation by collision occurs even at extremely low temperatures.

The 21-cm emission lines show that interstellar atomic hydrogen is strongly concentrated toward the galactic plane, and occurs in fairly discrete regions (clouds) in the spiral arms of our Galaxy. Galactic rotation broadens the line, in some cases as much as 800 kHz which corresponds to the radial velocity of about  $170 \text{ km s}^{-1}$ . The interstellar hydrogen in the path between some bright radio sources and the earth produces an absorption line superposed on the spectrum of the source. However, only a few sources are bright enough to permit such observations.

#### 22.6.2 Excited-State Hydrogen Lines

Emission lines of highly excited atomic hydrogen are observed in HII regions having high continuum temperatures. Transitions between energy levels of very large quantum number ( $n$ ) to the next lower quantum number ( $n-1$ ) have the highest probability. The emission line at 5009 MHz, transition  $n_{110} \rightarrow n_{109}$ , was detected in the Omega nebula (M17) and in the Orion nebula (M42). Lines at 1651.5 and 1715.7 MHz, corresponding to the transitions  $n_{159} \rightarrow n_{158}$  and  $n_{157} \rightarrow n_{156}$ , were found in M17 and W 51 (3C 400). Many other excited-state hydrogen lines in various HII regions probably will be reported in the next few years.

#### 22.6.3 The 18-cm Hydroxyl (OH) Lines

Figure 22-11 shows the energy levels for the 18-cm lines of the hydroxyl radical (OH), their frequencies, and theoretical relative intensities of the lines due to different transitions. These four energy levels result from hyperfine splitting of the two  $\Lambda$  doublets ( $J = 3/2$ ) of the ground state. The rest-frequencies of the lines are 1:5:9:1, respectively. The 1665 and 1667 MHz lines were discovered first as absorption lines in the radio spectrum of Cassiopeia A. All four were then found in the spectrum of Sagittarius A, but with anomalous intensity ratios (1:2.7:2.2:1).

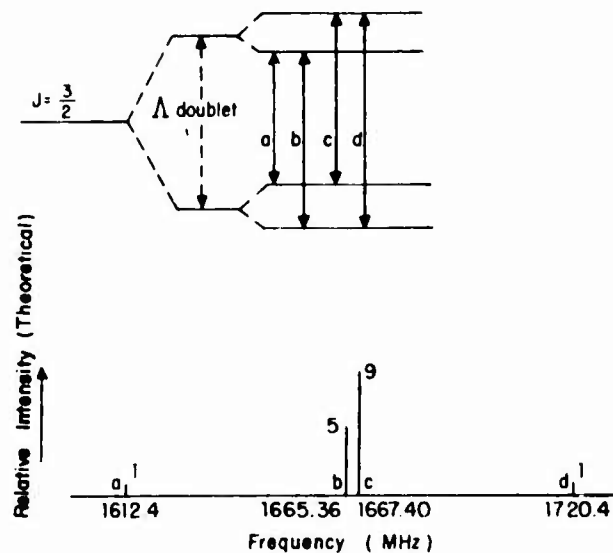


Figure 22-11. Energy levels, rest-frequencies, and relative line intensities (theoretical) for the  ${}^2\Pi_{3/2}$ ,  $J = 3/2$  state of OH

Observations reveal many peculiarities. The principle velocity components determined from the OH spectrum had no correlation whatever with the velocity components determined from the 21-cm hydrogen line in the same direction. Certain OH radiation is strongly linearly polarized, and some OH radiation, even from the same source, is strongly circularly polarized. At present, there is no satisfactory explanation of the observed phenomena; for an account of the various hypotheses, see Dieter and Goss [1966].

## 22.7 REFERENCES

- Carpenter, R. L., 1966, "Study of Venus by cw Radar - 1964 Results," *Astron. J.*, v. 71, p. 142.
- Conway, R. G., K. I. Kellermann, and R. J. Long, 1963, "The Radio Frequency Spectra of Discrete Radio Sources," *Monthly Notices Roy. Astron. Soc.*, v. 125, no. 3, p. 261.
- Dent, W. A., 1966, "Variation in the Radio Emission from the Seyfert Galaxy NGC 1275", *Astrophys. J.*, v. 144, no. 2, p. 843.
- Dieter, N. H. and W. M. Goss, 1966, "Recent Work on the Interstellar Medium", *Revs. Modern Phys.*, v. 38, no. 2, p. 256.
- Drake, F. D., 1964, "Microwave Observations of Venus 1962-63," *Astron. J.*, v. 69, no. 1, p. 62.

- Erickson, W.C. and W.M. Cronyn, 1965, "The Spectra of Radio Sources at Decametric Wavelengths," Astrophys. J., v. 142, no. 3, p. 1156.
- Evans, J.V., 1965, "Radar Studies of the Moon," Radio Science, v. 69D, no. 12, p. 1637.
- Guidice, D. A., 1966, "Spectra of Nine Discrete Sources in the 20 to 40 Mc/s Range," Nature, v. 211, p. 57.
- Howard, W.E., and S.P. Maran, 1965, "General Catalogue of Discrete Radio Sources," Astrophys. J., v. 10, Supplement no. 93, p. 1.
- Kellermann, K.I., 1966, "The Thermal Radio Emission from Mercury, Venus, Mars, Saturn, and Uranus," Icarus, v. 5, no. 5, p. 478.
- Lilley, A.E., P. Palmer, H. Penfield, and B. Zuckerman, 1966, "Radio Astronomical Detection of Helium," Nature, v. 211, p. 174.
- Mayer, C.H., 1964, "Thermal Radio Radiation from the Moon and Planets," IEEE Trans. Military Elect., v. MIL-8, p. 236, or IEEE Trans. Antennas and Propagation, v. AP-12, no. 7, p. 902.
- Pettengill, G.H. and R.B. Dyce, 1965, "A Radar Determination of the Rotation of the Planet Mercury," Nature, v. 206, p. 1240.
- Seeger, C.L., G. Westerhout, R.G. Conway, and T. Hoekema, 1965, "A Survey of the Continuous Radiation at a Frequency of 400 Mc/s," Bull. Astron. Inst. Netherlands, v. 18, p. 11.
- Tolbert, C.W., and A.W. Straiton, 1964, "35 Gc/s, 70 Gc/s and 94 Gc/s Cytherean Radiation," Nature, v. 204, p. 1242.
- Tolbert, C.W., 1966, "Observed Millimeter Wavelength Brightness Temperatures of Mars, Jupiter, and Saturn," Astron. J., v. 71, no. 1, p. 30.
- Troitsky, V.S., 1965, "Investigation of the Surfaces of the Moon and Planets by the Thermal Radiation," Radio Science, v. 69D, no. 12, p. 1585.
- Wild, J.P., 1966, "Instrumentation for Radio Astronomy," Physics Today, v. 19, no. 7, p. 28.

## Appendix B

### Blackbody Radiation

There is no single standard nomenclature for radiometric concepts. Terminology and symbols in different chapters of this handbook vary because those common in the literature for the particular topic are used. In each case, however, the concept is initially identified by the name given in Section B.1. Because different systems of units are also used, dimensions in Sec. B.2 and B.3 are given in mass (m), length (l), time (t), and unit solid angle ( $\Omega_0$ ). Formulas are for unpolarized blackbody radiation. For additional definitions and functions, and for a discussion of this nomenclature, see Pivovonsky and Nagel [1961], Planck [1912], and Bell [1959].

#### B.1 NOMENCLATURE, SYMBOLS, DEFINITIONS AND UNITS

The Systeme International (MKSA) units are used here, with the exceptions of wavelength interval, which is in microns, and wavenumber, which is in reciprocal centimeters.

Surface area,  $A$ , [ $m^2$ ].

Angle between normal to surface and direction of energy propagation,  $\theta$ , [rad].

Solid angle,  $d\Omega = 2\pi \sin\theta d\theta$ ;  $\Omega = 2\pi(1 - \cos\theta)$ , [sr].

Unit solid angle,  $\Omega_0$  is 1 steradian.

Radiant energy,  $U$ , [J].

$$\text{Radiant energy density, } u = \frac{1}{c} \int_0^{4\pi} N d\Omega, \quad [\text{J m}^{-3}].$$

$$\text{Radiant power, } P = dU/dt$$

$$= 2\pi \iint N dA \cos \theta \sin \theta d\theta, \quad [\text{W}].$$

$$\text{Radiance, } N = \frac{\partial^2 P}{\partial A \partial \Omega \cos \theta}, \quad [\text{W m}^{-2} \text{ sr}^{-1}].$$

Radiant emittance is radiant power per unit area emitted from a surface.

$$W = \int N d\Omega, \quad [\text{W m}^{-2}].$$

Irradiance (equivalent to the Poynting vector) is the radiant power per unit area incident on a surface element normal to the direction of energy

$$\text{propagation, } H = \frac{dP}{dA \cos \theta}, \quad [\text{W m}^{-2}].$$

Radiant intensity is the radiant power per solid angle from a point source,

$$J = \frac{dP}{d\Omega}, \quad [\text{W sr}^{-1}].$$

Frequency,  $\nu$ , [Hz].

Bandwidth,  $\Delta\nu$  or  $d\nu$ , [Hz].

Wavelength,  $\lambda$ , [m].

Wavelength interval (wavelength band),  $\Delta\lambda$  or  $d\lambda$ , [ $\mu$ ].

Wavenumber,  $\sigma$ , [ $\text{cm}^{-1}$ ].

Subscript  $\lambda$  indicates monochromatic radiation or radiation per wavelength interval, and the quantity is then called spectral, for example:

$u_\lambda$  is spectral energy density, [ $\text{J m}^{-3} \mu^{-1}$ ],

$W_\lambda$  is spectral radiant emittance, [ $\text{W m}^{-2} \mu^{-1}$ ].

Subscript  $\nu$  indicates radiation per bandwidth, for example:

$u_\nu$  is radiant energy density per bandwidth, [ $\text{J m}^{-3} \text{Hz}^{-1}$ ] or [ $\text{J sec m}^{-3}$ ],

$H_\nu$  is irradiance per bandwidth, [ $\text{W m}^{-2} \text{Hz}^{-1}$ ] or [ $\text{J m}^{-2}$ ].

Subscript  $\sigma$  indicates radiation per unit wavenumber, for example:

$N_\sigma$  is radiance per reciprocal centimeter [ $\text{W m}^{-2} \text{sr}^{-1} (\text{cm}^{-1})^{-1}$ ] or [ $\text{W cm m}^{-2} \text{sr}^{-1}$ ].

## B.2 PLANCK'S RADIATION FUNCTIONS

Planck's law for the energy per unit volume of unpolarized blackbody radiation of frequency  $\nu$  is

$$u_\nu = \frac{8\pi h\nu^3}{c^3 [\exp(h\nu/kT) - 1]} \quad (B-1)$$

where  $T$  is the temperature of the blackbody in  $^{\circ}\text{K}$ ,  $h$  is Planck's constant,  $k$  is Boltzmann's constant, and  $c$  the speed of propagation. (For plane polarized radiation, divide formulas by 2; e.g., for  $u_\nu$ , the numerator would be  $4\pi h\nu^3$ .) From Eq. (B-1) and the relationships

$$u_\lambda = u_\nu c/\lambda^2, \quad (B-2)$$

and

$$u = \int_0^\infty u_\lambda d\lambda = \int_0^\infty u_\nu d\nu, \quad (B-3)$$

many different functions are obtained.

The formulas that follow are used for various applications in this handbook. The second radiation constant,  $c_2$ , is used in wavelength equations; the "first radiation constant" is not used because there is no commonly accepted definition (Planck uses  $hc^2/\Omega_0$ ; other forms found in the literature are  $8\pi hc$ ,  $\pi hc^2$ ,  $2\pi hc^2$ , and  $2hc^2/\Omega_0$ , with correspondingly different numerical values quoted).

$$\begin{aligned} u_\lambda &= 8\pi hc \lambda^{-5} [\exp(c_2/\lambda T) - 1]^{-1} \quad [m \ell^{-2} t^{-2}], \\ N_\nu &= 2 h\nu^3 c^{-2} \Omega_0^{-1} [\exp(h\nu/kT) - 1]^{-1} \quad [m t^{-2} \Omega_0^{-1}], \\ N_\lambda &= 2 hc^2 \Omega_0^{-1} \lambda^{-5} [\exp(c_2/\lambda T) - 1]^{-1} \quad [m \ell^{-1} t^{-3} \Omega_0^{-1}], \\ N_\sigma &= 2 hc^2 \sigma^3 \Omega_0^{-1} [\exp(c_2 \sigma/T) - 1]^{-1} \quad [m \ell t^{-3} \Omega_0^{-1}], \\ W_\nu \text{ (or } H_\nu) &= 2 h\nu^3 c^{-2} [\exp(h\nu/kT) - 1]^{-1} [m t^{-2}], \\ W_\lambda \text{ (or } H_\lambda) &= 2 hc^2 \lambda^{-5} [\exp(c_2/\lambda T) - 1]^{-1} [m \ell^{-1} t^{-3}]. \end{aligned} \quad (B-4)$$

Figures B-1 through B-4 show  $N_\lambda$ ,  $N_\sigma$ , and  $N_\nu$  for blackbodies at various temperatures as a function of  $\lambda$ ,  $\sigma$ , and  $\nu$ . Figures B-5 through B-7 are plots of the number of photons of a given wavelength, wavenumber, or frequency, emitted per unit area per unit solid angle by a blackbody at various temperatures. In plotting these curves, the values  $c_2 = 1.4380 \text{ cm } ^{\circ}\text{K}$ ,  $2hc^2/\Omega_0 = 1.1909 \times 10^{-12}$

$\text{W cm}^2 \text{sr}^{-1}$ , and for Wien's displacement constant  $0.28962 \text{ cm } ^\circ\text{K}$ , were used; the values recommended by the National Bureau of Standards were published after calculations were completed.

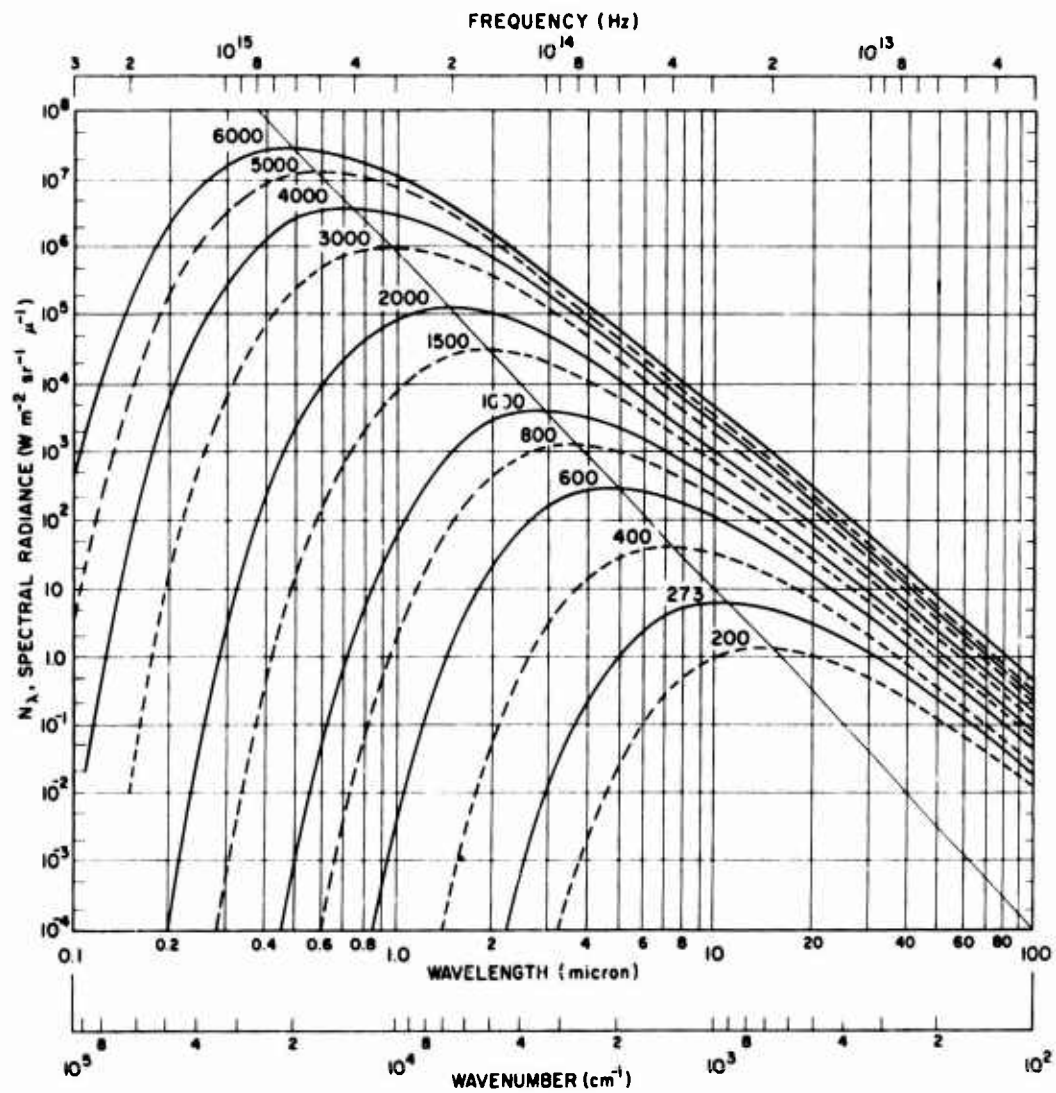


Figure B-1. Spectral radiance of a blackbody,  $N_\lambda$ , at the temperature in  $^\circ\text{K}$  shown on each curve; beyond  $100 \mu$  the curves continue to be linear (plotted on logarithmic scales). The diagonal line, intersecting the curves at their maxima, shows Wien's displacement law. (Subdivisions of the ordinate scale are at 2 and 5.) Figure by P. R. Gast.

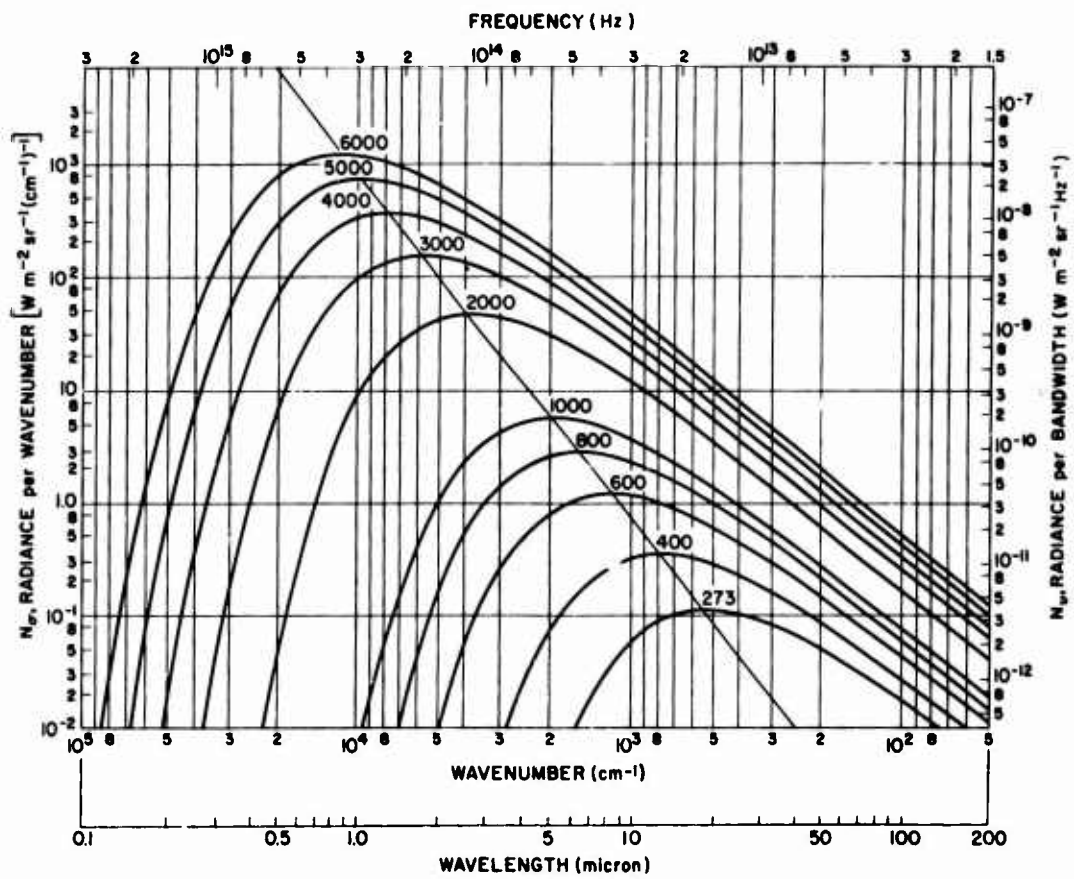


Figure B-2. Radiance per reciprocal centimeter,  $N_0$ , and radiance per unit frequency,  $N_\lambda$ , for a blackbody at various temperatures; at frequencies less than  $3 \times 10^{12}$  Hz, wavenumber  $< 100 \text{ cm}^{-1}$ , the curves continue to be linear (plotted on logarithmic scales). The diagonal line, intersecting the curves at their maxima, shows Wien's displacement law. Figure by P. R. Gast.

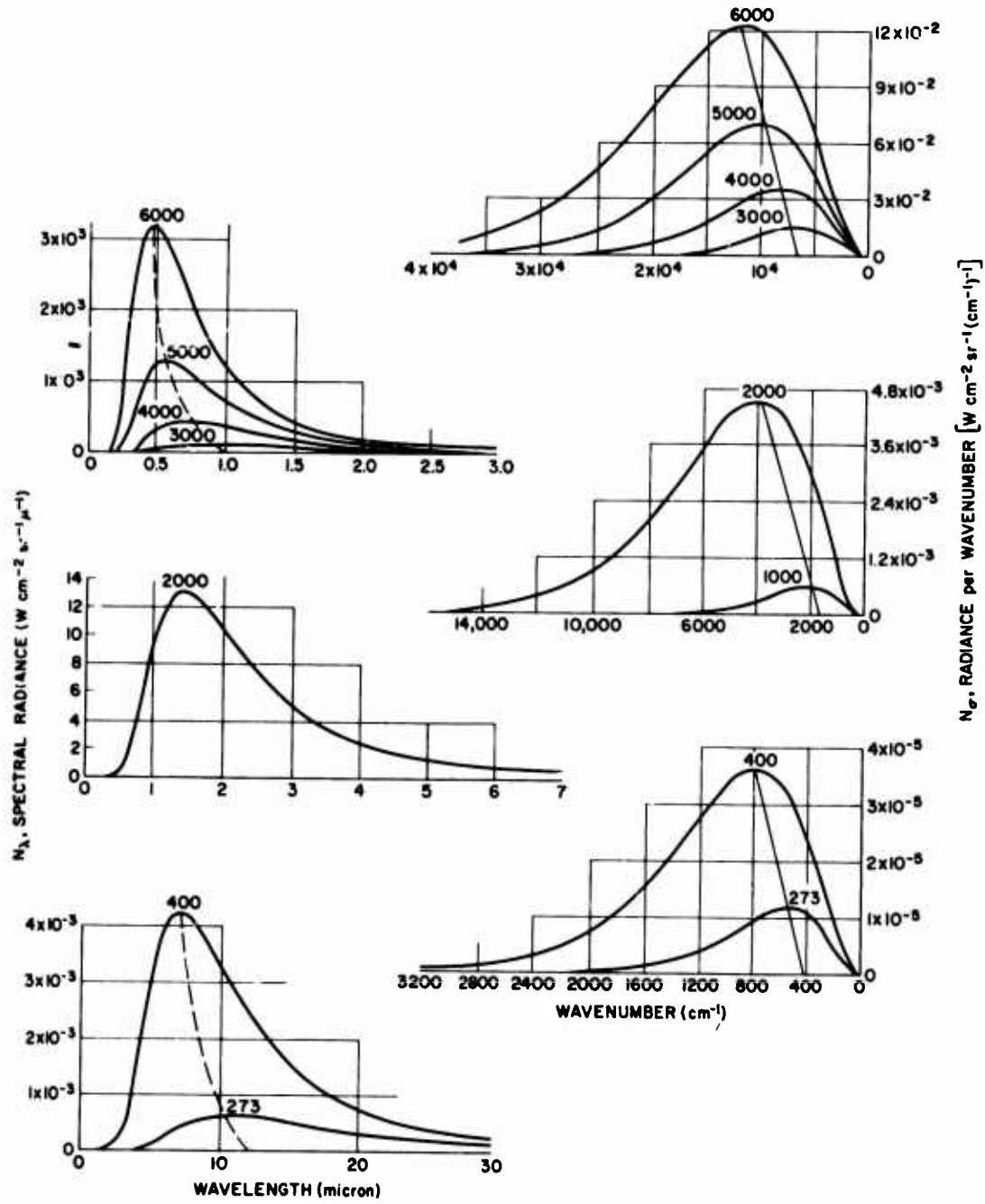


Figure B-3. Spectral radiance  $N_\lambda$  and radiance per reciprocal centimeter  $N_\nu$  of blackbodies at various temperatures ( $^\circ K$ ) plotted on arithmetic scales; note values given are per square centimeter of surface and must be multiplied by  $10^4$  to obtain values in  $W\ m^{-2}\ sr^{-1}\ \mu^{-1}$  or  $W\ m^{-2}\ sr^{-1}\ (cm^{-1})^{-1}$ . The dashed and diagonal lines show Wien's displacement law. Figure by P.R. Gast.

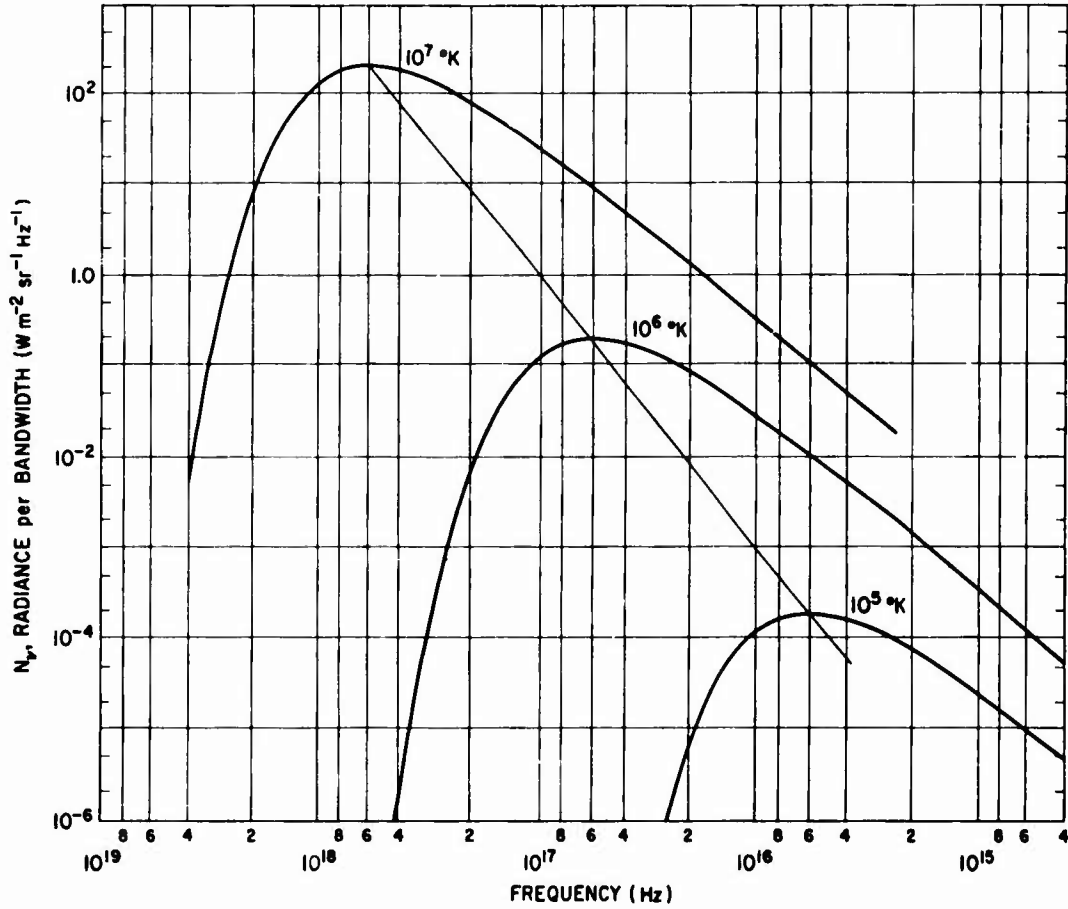


Figure B-4. Radiance per unit frequency,  $N_\lambda$ , for blackbodies at high temperatures vs frequency (wavelength region  $0.75 \text{ \AA}$  to  $0.75 \mu$ ). The diagonal line shows Wien's displacement law. Subdivisions of ordinate scale are at 2 and 5. Figure by P. R. Gast.

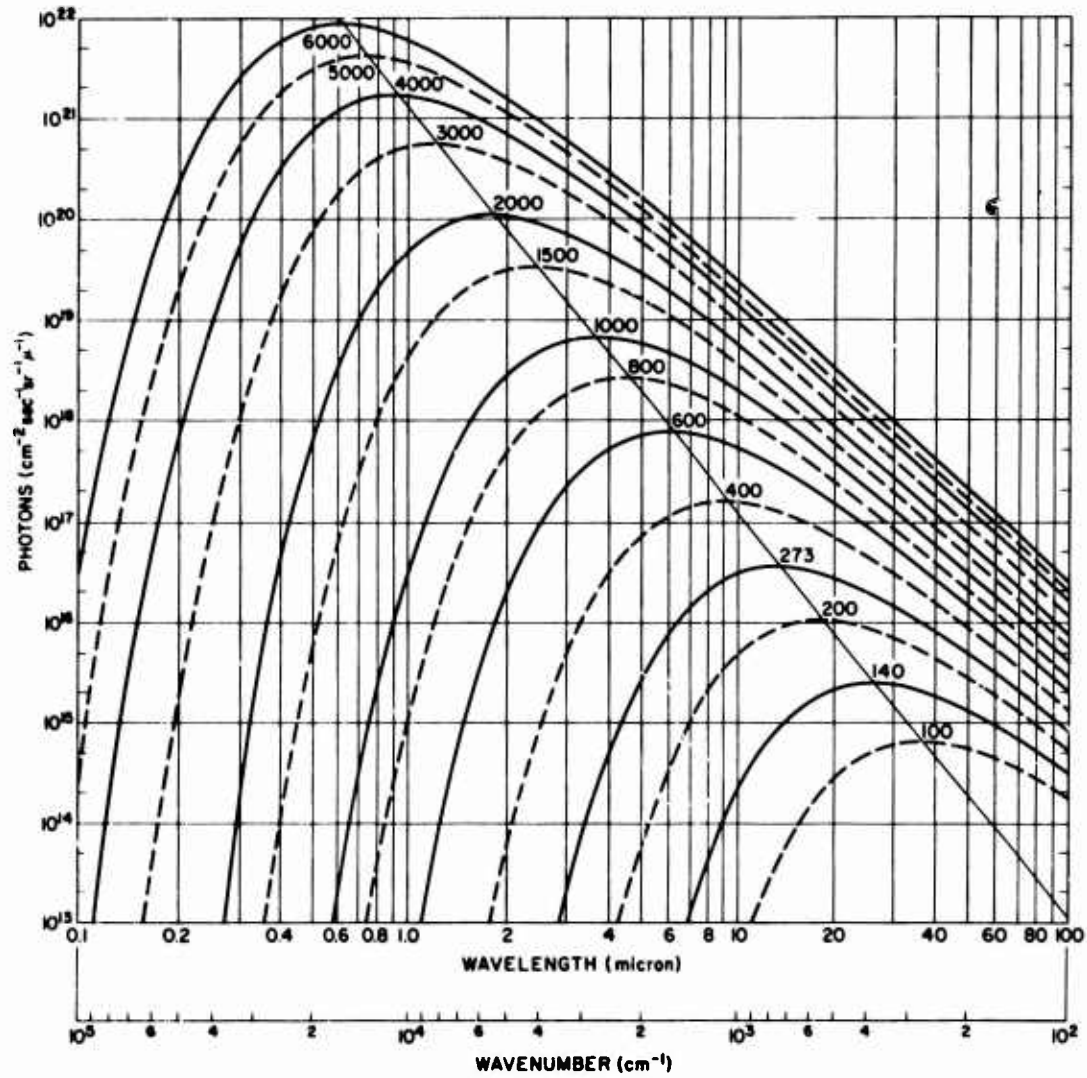


Figure B-5. Number of photons per second emitted per square centimeter per steradian per micron by a blackbody at various temperatures (°K); subdivisions of the ordinate scale are at 2 and 5. The diagonal line, intersecting the curves at their maxima, shows Wien's displacement law. Figure by P. R. Gast.

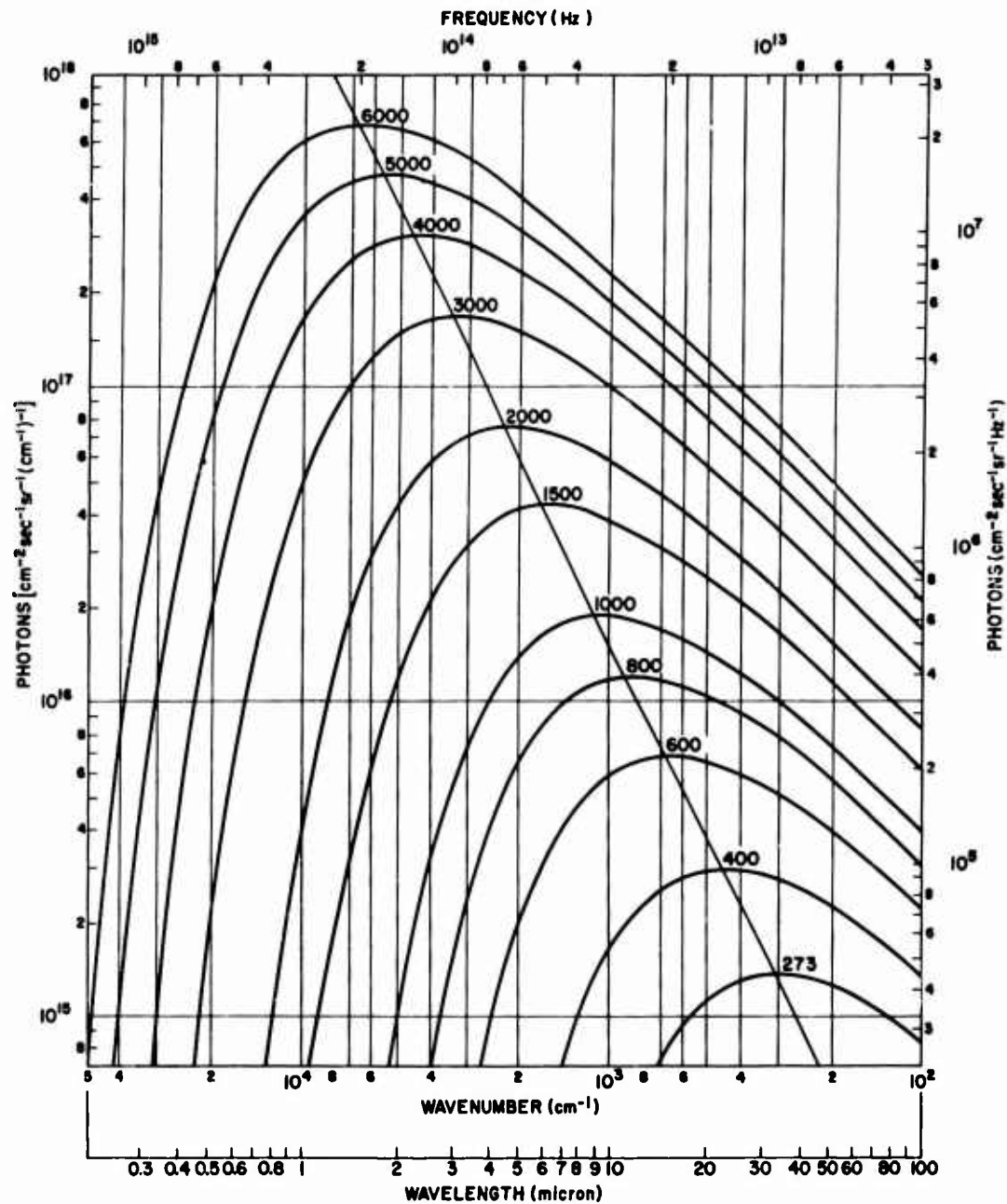


Figure B-6. Number of photons per second per square centimeter per steradian per reciprocal centimeter (left ordinate scale) and number of photons per second per square centimeter per steradian per unit frequency (right ordinate scale) emitted by a blackbody at various temperatures ( $^{\circ}\text{K}$ ). The diagonal line, intersecting the curves at their maxima, shows Wien's displacement law. Figure by P. R. Gast.

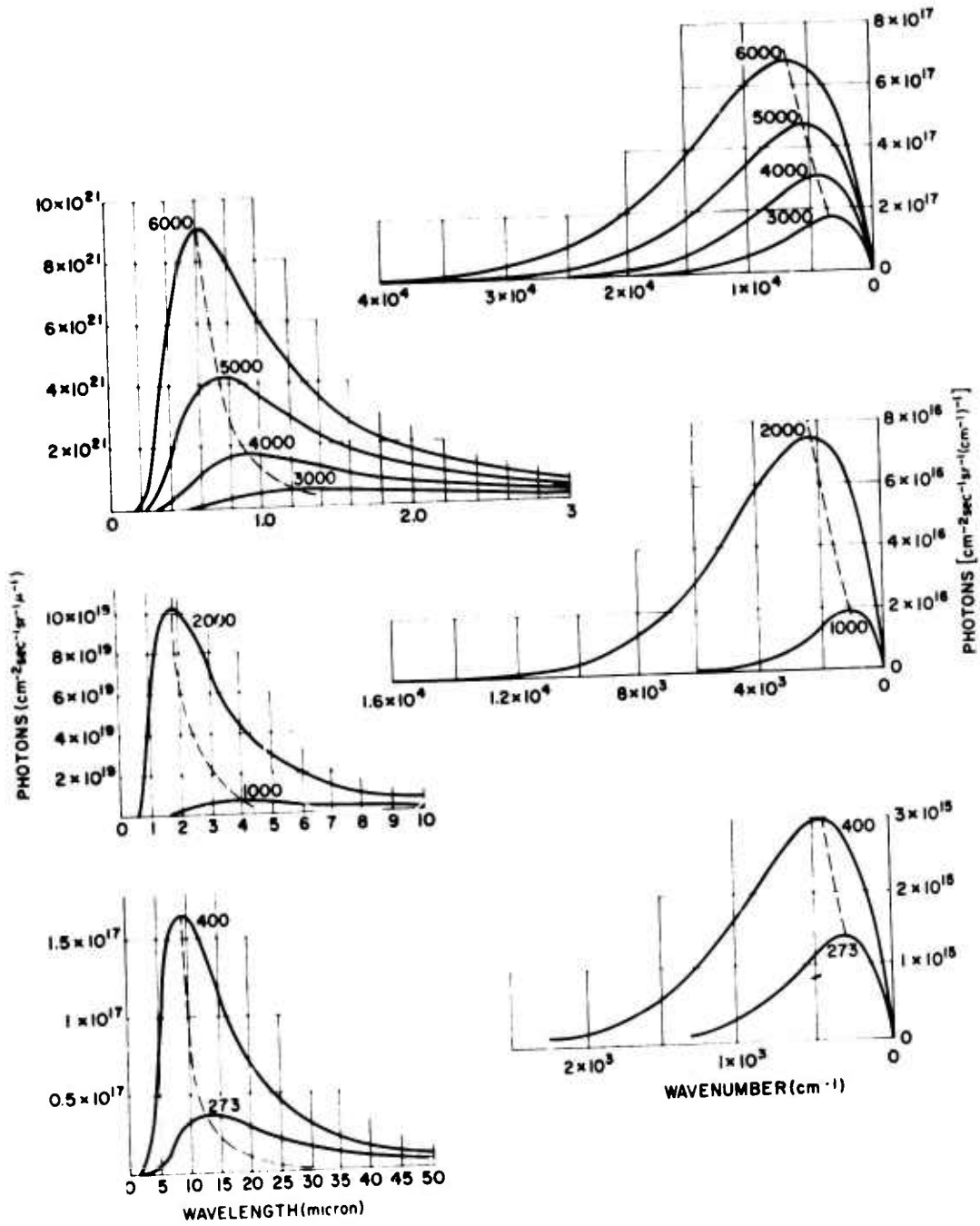


Figure B-7. Photons per second emitted by blackbodies at various temperatures (°K) plotted on arithmetic scales. Figure by P.R. Gast.

### B.3 LIMITING CASES OF PLANCK'S LAW

Two approximations of Eq. (B-1) are the Rayleigh-Jeans and the Wien radiation formulas.

The Rayleigh-Jeans approximation is applicable to low-frequency, long-wavelength radiation (radio region) where  $h\nu \ll kT$ . A few of the forms are:

$$\begin{aligned}
 u_\nu &= 8\pi\nu^2 kT c^{-3} \\
 u_\lambda &= 8\pi kT \lambda^{-4} \\
 N_\nu &= 2\nu^2 kT c^{-2} \Omega_0^{-1} \\
 N_\lambda &= 2ckT \Omega_0^{-1} \lambda^{-4} \\
 N_\sigma &= 2c\sigma^2 kT \Omega_0^{-1} \\
 W_\nu \text{ (or } H_\nu) &= 2\nu^2 kT c^{-2} \\
 W_\lambda \text{ (or } H_\lambda) &= 2ckT \lambda^{-4} .
 \end{aligned}
 \tag{B-5}$$

The Wien radiation function is useful for high-frequency, short-wavelength radiation where  $h\nu \gg kT$ . Formulas are:

$$\begin{aligned}
 u_\nu &= 8\pi h\nu^3 c^{-3} \exp(-h\nu/kT) , \\
 u_\lambda &= 8\pi hc \lambda^{-5} \exp(-c_2/\lambda T) , \\
 N_\nu &= 2h\nu^3 c^{-2} \Omega_0^{-1} \exp(-h\nu/kT) , \\
 N_\lambda &= 2hc^2 \Omega_0^{-1} \lambda^{-5} \exp(-c_2/\lambda T) , \\
 N_\sigma &= 2hc^2 \sigma^3 \Omega_0^{-1} \exp(-c_2\sigma/T) , \\
 W_\nu \text{ (or } H_\nu) &= 2h\nu^3 c^{-2} \exp(-h\nu/kT) , \\
 W_\lambda \text{ (or } H_\lambda) &= 2hc^2 \lambda^{-5} \exp(-c_2/\lambda T) .
 \end{aligned}
 \tag{B-6}$$

### B.4 STEFAN-BOLTZMANN AND WIEN DISPLACEMENT LAWS

The Stefan-Boltzmann law states that the total energy density of blackbody radiation depends only on the temperature of the body;  $u = aT^4$ . (The constant of the proportionality,  $a$ , is  $8\pi^5 k^4 / 15 c^3 h^3$ .) Thus the radiant emittance of a blackbody is

$$W = \frac{c}{4\pi} a T^4 = \sigma T^4 ; \quad (B-7)$$

$\sigma$  is the Stefan-Boltzmann constant.

Wien's displacement law is usually given in the form

$$\lambda_{\max} T = c_2 / r_\lambda = 2.8978 \times 10^{-3} \text{ [ m }^\circ\text{K] } , \quad (B-8)$$

where  $\lambda_{\max}$  is the wavelength at which the spectral radiant emittance is maximum ( $dW_\lambda/d\lambda = 0$ ),  $r_\lambda$  is the positive root of the equation  $x = 5 [1 - \exp(-x)] = 4.9651$  and  $2.8978 \times 10^{-3}$  is Wien's displacement constant. Two forms which are less common but for some purposes more useful are:

frequency at which the energy is maximum ( $dH_\nu/d\nu = 0$ ),

$$\nu_{\max} = r_\nu kT/h = 5.8820 \times 10^{10} T \text{ [ Hz ] } ; \quad (B-9)$$

wavelength at which the energy is maximum ( $dH_\nu/d\lambda = 0$ ),

$$\lambda_{\nu_{\max}} T = \frac{c T}{\nu_{\max}} = c_2 / r_\nu = 5.0968 \times 10^{-3} \text{ [ m }^\circ\text{K] } , \quad (B-10)$$

where  $r_\nu$  is the positive root of the equation  $x = 3 [1 - \exp(-x)] = 2.8214$ . Note that for a given temperature, the maximum of the energy distribution spectrum is not the same as the maximum of the conventional spectral distribution (spectral radiant emittance vs wavelength).

### B.5 REFERENCES

- Bell, Ely E., 1959, "Radiometric Quantities, Symbols and Units," Proc. IRE, v. 47, no. 9, p. 1432.
- Pivovonsky, M., and M.R. Nagel, 1961, "Tables of Blackbody Radiation Functions," The Macmillan Co., New York.
- Planck, Max, 1912, "Theory of Heat Radiation," authorized translation, reprinted by Dover Publications, Inc., New York, 1959.

Unclassified  
Security Classification

DOCUMENT CONTROL DATA - R&D		
<i>(Security classification of title, body of abstract and indexing annotation must be entered when the overall report is classified)</i>		
1. ORIGINATING ACTIVITY <i>(Corporate author)</i> Air Force Cambridge Research Laboratories (ECS) L.G. Hanscom Field Bedford, Massachusetts 01730		2a. REPORT SECURITY CLASSIFICATION Unclassified
		2b. GROUP
3. REPORT TITLE RADIO ASTRONOMY: A REVISION OF CHAPTER 22 OF THE HANDBOOK OF GEOPHYSICS AND SPACE ENVIRONMENTS		
4. DESCRIPTIVE NOTES <i>(Type of report and inclusive dates)</i> Scientific. Summary.		
5. AUTHOR(S) <i>(First name, middle initial, last name)</i> D. A. Guidice		
6. REPORT DATE November 1967	7a. TOTAL NO. OF PAGES 56	7b. NO. OF REFS 18
8a. CONTRACT OR GRANT NO. .	9a. ORIGINATOR'S REPORT NUMBER(S) AFCRL-67-0621	
b. PROJECT, TASK, WORK UNIT NOS. None		
c. DOD ELEMENT	9b. OTHER REPORT NO(S) <i>(Any other numbers that may be assigned this report)</i>	
d. DOD SUBELEMENT	AFSG No. 199	
10. DISTRIBUTION STATEMENT 1-Distribution of this document is unlimited. It may be released to the Clearinghouse, Department of Commerce, for sale to the general public.		
11. SUPPLEMENTARY NOTES TECH, OTHER	12. SPONSORING MILITARY ACTIVITY Air Force Cambridge Research Laboratories (ECS) L.G. Hanscom Field Bedford, Massachusetts 01730	
13. ABSTRACT This survey is a summary of available information on radiation environments at radio frequencies (about 10 m to 1 cm wavelength); the Moon, the Planets, and space beyond the solar system are described. The topics presented are refraction and absorption of extraterrestrial radio waves by Earth's atmosphere, radio and radar observations of the Moon and Planets, radio emission from the celestial sphere (background radiation), discrete sources of continuum radio emission, and spectral-line radiation from neutral atomic hydrogen and from the hydroxyl radical (OH).		

DD FORM 1473  
1 NOV 65

Unclassified  
Security Classification

Unclassified

Security Classification

14.	KEY WORDS	LINK A		LINK B		LINK C	
		ROLE	WT	ROLE	WT	ROLE	WT
	Radio Astronomy Radio Emission from Moon and Planets Radar Observations of Moon and Planets Radio Sources, Celestial						

Unclassified

Security Classification